JGR Biogeosciences

RESEARCH ARTICLE
10.1029/2018JG004628

Modeling Transient Soil Moisture Limitations on Microbial Carbon Respiration

Yuchen Liu[1], Corey R. Lawrence[2], Matthew J. Winnick[3,4], Hsiao-Tieh Hsu[3], Katharine Maher[3,5], and Jennifer L. Druhan[1]

[1]Department of Geology, University of Illinois at Urbana–Champaign, Champaign, IL, USA, [2]Geologic & Environmental Change Science Center, U. S. Geological Survey, Denver, CO, USA, [3]Department of Earth System Science, Stanford University, Stanford, CA, USA, [4]Department of Geosciences, University of Massachusetts Amherst, Amherst, MA, USA, [5]Rocky Mountain Biological Laboratory, Crested Butte, CO, USA

Key Points:
- Soil incubation results exhibit a transient response in soil carbon respiration rates after a wetting event (the Birch effect)
- Two models with different structures and levels of complexity (first-order and dormancy-incorporated) were tested against two sets of data with distinct spatial and temporal resolution
- The dormancy-incorporated model achieves statistically favorable values while simulating incubation data for soil samples taken above ~100 cm, and the first-order model achieves better AIC values when simulating deeper soil samples, which comprise a minor portion of the overall CO_2 flux

Supporting Information:
- Supporting Information S1
- Figure S1

Correspondence to:
Y. Liu,
liu305@illinois.edu;
jdruhan@illinois.edu

Citation:
Liu, Y., Lawrence, C. R., Winnick, M. J., Hsu, H.-T., Maher, K., & Druhan, J. L. (2019). Modeling transient soil moisture limitations on microbial carbon respiration. *Journal of Geophysical Research: Biogeosciences*, *124*, 2222–2247. https://doi.org/10.1029/2018JG004628

Received 25 MAY 2018
Accepted 13 JUN 2019
Accepted article online 2 JUL 2019
Published online 22 JUL 2019

©2019. American Geophysical Union. All Rights Reserved.

Abstract Soil microorganisms are known to survive periods of aridity and to recover rapidly after wetting events, with the ability to transition between a dormant state in dry conditions and an active state in wet conditions. Though this dynamic behavior has been previously incorporated into soil carbon respiration modeling frameworks, a direct comparison between this active-dormant transition mechanism and a more simplified first-order model has yet to be made. Here, we demonstrate the necessary extent of model complexity needed to reproduce transient carbon respiration rates obtained from a set of soil incubation experiments implemented over a range of soil depths and time intervals. Two approaches are tested, one uses simplified first-order kinetics, whereas the other employs a transition between active and dormant biomass. The performance of each model is evaluated using an Akaike Information Criterion (AIC) based on the accuracy with which they reproduce an experimental dataset consisting of two sets of time series soil incubations collected across a range of time and depth resolutions. Based on the AIC evaluation and model-data comparison, we conclude that a dormancy-enabled model featuring two distinct microbial strategists performs best for the majority of the soil profile (above 108 cm) for both high and low depth resolution and sampling frequency, despite the added parameters required. In contrast, the first-order model achieves better AIC scores when simulating our deepest soils (112–165 cm), where moisture fluctuations are expected to be less prevalent. These results guide how and where we choose to apply more cost intensive models.

Plain Language Summary Microorganisms in the soil environment respire substantial amounts of CO_2, comprising an important flux of carbon to the atmosphere and playing a key role in moderating carbon storage. We seek to improve our ability to model the amount of CO_2 emitted from soil by evaluating two modeling frameworks against lab-measured respiration rates using natural soil samples at a range of soil moistures. Results show that a simplified model is more suitable for interpreting the soil respiration rates below 100 cm, while a more complex simulation of the activity of microbes as a function of soil moisture is necessary for shallower depths.

1. Introduction

Soils are one of the largest reservoirs of terrestrial carbon at the Earth's surface and thus represent a significant potential source of CO_2 to the atmosphere via heterotrophic and autotrophic respiration (Batjes, 1996; Bellamy et al., 2005). Previous studies have shown that a wide variety of parameters can influence the rate of soil carbon respiration, including temperature (Lloyd & Taylor, 1994; Kirschbaum, 1995; Rey et al., 2005; Pekka Vanhala et al., 2008; Niklińska & Klimek, 2007; Lellei-Kovács et al., 2016), microbial community composition (Monson et al., 2006; Cleveland et al., 2007; Y. Li et al., 2006; P. Vanhala et al., 2005; Kant et al., 2011), pH (Bååth & Anderson, 2003; Pekka Vanhala, 2002), soil organic carbon composition (Cross & Sohi, 2011; Sanaullah et al., 2012), soil texture (X. Li et al., 2015), and soil moisture (Howard & Howard, 1993; Jia et al., 2007; Orchard & Cook, 1983; Wagle & Kakani, 2014).

Among these factors, the pronounced influence of water availability (soil moisture) on CO_2 production within soil profiles potentially results in a direct feedback between the hydrologic cycle and the carbon cycle. Quantifying this relationship is vital to the prediction of carbon cycle dynamics in a changing climate (Luo

et al., 2016). Many studies across a wide range of settings have demonstrated a positive correlation between soil respiration rate and moisture in arid and semiarid systems, and a negative correlation in soils approaching saturation, with a peak in between (Davidson et al., 1998; Einola et al., 2007; Elberling, 2003; Euskirchen et al., 2003; Falk et al., 2005; Grant & Rochette, 1994; Grundmann et al., 1995; Hao et al., 2016; Harmon, 2009; Harmon et al., 2011; Howard & Howard, 1993; Husen et al., 2014; Jin et al., 2008; Kang et al., 2003; Mielnick & Dugas, 2000; Moncrieff & Fang, 1999; Pumpanen et al., 2003; Reichstein et al., 2003; Rey et al., 2005; Tian et al., 2010; Verburg et al., 2005; X. Wang et al., 2010). When soils approach full water saturation, pore wet-up and blockage combine to constrain the availability of oxygen by limiting the diffusion rate (Cook & Knight, 2003; Grant & Rochette, 1994; Skopp et al., 1990), resulting in diminished total respiration across intact soil cores (Gabriel & Kellman, 2014). The factors contributing to reduced respiration rates at low soil moisture contents are less clear. Two processes have been suggested to describe this response. First, the availability of accessible bioavailable carbon indirectly affects microbial activity as a result of decreased water connectivity as soil pores dry, which hinders the transport of dissolved organic matter and other nutrients (Blazewicz et al., 2014; Eric A. Davidson et al., 2014; Schjønning et al., 2003; Skopp et al., 1990). Relatedly, some studies have suggested that the soil moisture-respiration relationship could stem from decreased organic carbon addition to soils via root exudates in drier conditions (Canarini & Dijkstra, 2015; Gorissen et al., 2004; Persson et al., 1995). The second process involves a direct limitation on respiration rate as a result of dormancy triggered by a decrease in soil moisture as a survival mechanism. Such a reduction of active microbial biomass capable of respiration thus results in an overall slower metabolism and reduced soil carbon respiration rates (Brockett et al., 2012; Lennon & Jones, 2011; S. Manzoni et al., 2014; Stevenson, 1977; G. Wang et al., 2015).

The response of soil respiration rates to wetting events is also a transient feature. When soils are rewet after a prolonged period of dry conditions, it is common to observe a large pulse of CO_2 followed by a decrease to lower, steady state values (Werner Borken & Matzner, 2009; Inglima et al., 2009; Kim et al., 2010; Wu & Lee, 2011). This observation is commonly referred to as the Birch effect (Birch, 1958, 1960, 1964). The validity of the Birch effect has been suggested in both controlled incubation (Göransson et al., 2013; Kieft et al., 1987; Shi & Marschner, 2014; Unger et al., 2010) and field-scale systems (Cable et al., 2008; Xu et al., 2004; Yan et al., 2014). A recent study by Fan et al. (2015) demonstrated that this initial pulse can represent a major component of the total carbon respiration flux from soils; however, few models are designed to capture this behavior. As increasingly high-resolution depth and time records of CO_2 respiration and terrestrial fluxes are reported (e.g., Carbone et al., 2011; Davidson et al., 2012; Xu et al., 2004), these observations highlight the uncertainty in the choice of appropriate model at each resolution and the extent to which they are related or can be resampled across scales.

A wide variety of explanations for the Birch effect have been proposed. Among these, several studies have suggested extracellular enzymes (exoenzymes) produced by microbes for the purpose of solubilizing complex carbon to readily metabolized compounds remain active even in dry conditions (Blankinship et al., 2014). As a result, low molecular weight carbon accumulates during dry periods, leading to an initially high concentration when soil moisture rises again (Iovieno & Bååth, 2008; Lawrence et al., 2009; S. Manzoni et al., 2014; Meisner et al., 2015; Miller et al., 2005), and furthermore, a longer period of dry conditions results in the accumulation of soluble carbon.

In addition, different microbial communities exhibit unique optimal effective saturation ranges (Barnard et al., 2013; Barnard et al., 2015; Evans & Wallenstein, 2014; Lauber et al., 2013). This observation implies, for example, that a microbial population which is active at a low soil moisture may be dormant at higher moisture, leading to distinct activated microbial communities in the same soil sample. Moreover, the rate of activation following a change in effective saturation is unique to each microbial population (Blagodatskaya & Kuzyakov, 2013; Martiny et al., 2013; Placella et al., 2012; Schimel & Schaeffer, 2015). Previous studies have shown that microbial populations characterized by a slower reproduction rate and higher energy efficiency are more optimally suited to environments with relatively stable physical parameters (e.g., soil moisture) and nutrient sources, while highly transient systems support microbial populations capable of pulses of rapid, energy-inefficient growth (Andrews & Harris, 1986; Dorodnikov et al., 2009).

In total, these studies illustrate a suite of complex and highly coupled relationships between the hydrology, microbiology, and carbon dynamics of soils. As a result, a wide variety of models have been developed for

soil respiration as a function soil moisture (Abramoff et al., 2017; Chen et al., 2011; Hashimoto & Komatsu, 2006; Lawrence et al., 2009; Stefano Manzoni et al., 2012; F.E. Moyano et al., 2012; Fernando E. Moyano et al., 2013; Paul et al., 2003; Tian et al., 2010; Welsch & Hornberger, 2004). These approaches have involved a broad diversity of structures in the effort to achieve a more robust approach appropriate to a variety of soil types and locations.

For example, Oikawa et al., (2014) used a modified Dual Arrhenius Michaelis-Menten kinetic rate expression that incorporates two carbon pools (labile and recalcitrant) as a means of fitting their observed surface CO_2 flux data. They successfully simulated a transient pulse in respiration due to a wetting event with the assumption of low soluble carbon concentrations prior to rewetting. While the introduction of an extra carbon pool increased their model complexity, the approach greatly improved prediction of the Birch effect. However, this method would be incompatible with systems in which labile carbon substantially accumulates during dry periods as described above.

Modeling structures such as that utilized by Oikawa et al., (2014) thus offer improved simulation of surface CO_2 flux, under conditions where labile carbon buildup between pulses is minimal. When this assumption is not warranted, an alternative framework may be required. For example, by explicitly tracking changes in microbial activity with shifts in soil moisture, the response in microbial respiration rate resulting from changes in environmental conditions can provide a moisture sensitivity feedback (Blagodatskaya & Kuzyakov, 2013) without restricting carbon buildup. Here, we evaluate the performance of a process-based approach with such simulation capacity adapted from Manzoni et al. (2014), in comparison to a simpler first-order respiration model. We will subsequently return to the application and functionality of these alternative model structures in comparison to our own design later in the paper (section 4.1). Both models were calibrated using CO_2 respiration rates obtained from a set of incubation experiments, using the shallow depth of a soil column collected from the East River watershed located near the Rocky Mountain Biological Laboratory, Colorado, USA. The calibrated models with optimal parameter sets were then applied to each depth of the same soil profile. Due to the different number of parameters used in the two models, the Akaike Information Criterion (referred to as AIC; Akaike, 1998) was applied to quantitatively evaluate the two models with the consideration of both the number of parameters used and the precision of the simulation.

2. Materials and Methods

2.1. Sample Collection

Soil samples were collected in the upper East River watershed within the Gunnison River Basin, located near Crested Butte, Colorado, USA (Figure 1). The upper East River is a high montane watershed with an average elevation of 3,350 m and stream flow dominated by snowmelt in spring and summer. The amount of snowmelt is approximately equal to the total water demand of this region, including atmospheric evaporation, plant uptake, and drainage into the groundwater and river network (Markstrom & Hay, 2009).

The sampling site for the current study is underlain by the calcareous shale from the Cretaceous Mancos Shale Formation, with colluvial sediments at the surface, ~3.5 km northwest of Rocky Mountain Biological Laboratory. The predominant vegetation in this section of the catchment is subalpine meadow. The sampling site has a seasonal drainage environment with little or no slope, with an average annual temperature of 1 °C and an average precipitation of 1.23 $\pm$ 0.26 m/year driven by both an annual monsoon season (~20% of total precipitation) and as snowfall (Winnick et al., 2017). Though precipitation predominantly occurs in the winter and spring months, local soil moisture is significantly affected by summer monsoon rainfall (Harte et al., 1995), which may result in a Birch Effect type respiration response.

The principle properties of the soil horizons were directly recorded during sampling (Table S1 in the supporting information). Two batches of samples were collected on different sampling expeditions in a subalpine meadow along Bradley Creek, a tributary of the East River. The first collection was conducted in November 2015 when three samples were taken at a coarse resolution of ~50-cm intervals from a hand-augured hole to a maximum depth of 165 cm. The shallow sample (0–52 cm) is primarily a mixture of the A1 and A2 horizon, the intermediate sample (63–108 cm) represents a mixture of horizons A/B, B/C, and Cw1, and the deep sample (112–165 cm) contains soil from the Cw2 horizon. The second set of samples

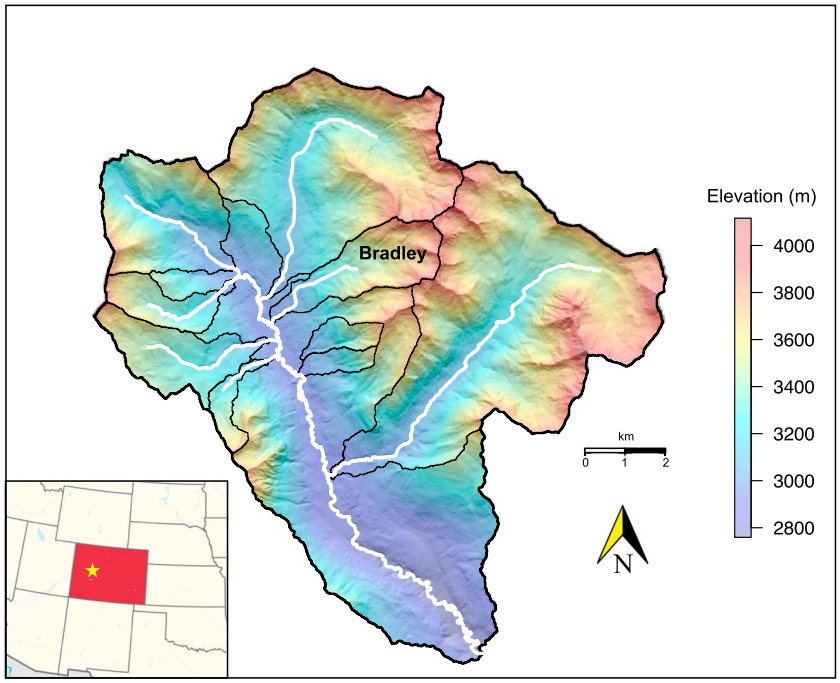


Figure 1. The East River watershed within the Gunnison River basin, Colorado, USA (the drainage paths are shown in white line). The red star illustrates the location where the soil incubation samples were collected for the current study (38°59′8.42″N, 107°0′12.51″W).

was collected in June 2016 from a soil pit located within 3 m of the original sampling location. During sampling of the soil pit, basic soil characteristics were recorded and additional samples were collected with 10-cm depth interval, to a maximum depth of 50 cm. These five samples represent the mixture of OA and A1 horizon (0–10 cm), A1 (10–20 and 20–30 cm), the mixture of A1 and A2 (30–40 cm), and A2 (40–50 cm). This second collection of samples was incubated both individually and aggregated to recreate the shallow sample of the first collection (detailed description shown in section 2.4.2). Immediately upon each collection, samples were sealed in plastic bags and kept under cool, dark conditions until processing could be completed. Prior to incubations, all soils were air dried for 2 weeks at ambient temperature (22 °C) before they were crushed and sieved to 2 mm to remove the coarse fraction, consisting of large stones and biological material.

2.2. Effective Saturation

Water-holding capacity was determined by wetting three 10-g subsamples of air-dried soils gradually until they became fully saturated. Samples were weighed before and after water addition to quantify the mass needed for the soils to fully saturate for all three subsamples. The average of the three numbers was used as the final saturated value with a standard deviation smaller than 5% of the water mass, where the air-dried samples are considered 0% (Sat_{residual}), and 100% represents full saturation (Sat_{sat}). These values are subsequently reported as effective saturation (Se, defined as $(Sat_{\mathrm{sample}} - Sat_{\mathrm{residual}})/(Sat_{\mathrm{sat}} - Sat_{\mathrm{residual}})$) for the remainder of the paper.

2.3. Soil Carbon Content

Elemental analysis (EA) was used to determine the amount of carbon in the coarsely sampled soil collected at ~50-cm-depth intervals prior to incubations. All EA measurements were performed using the Carlo-Erba NA 1500 analyzer (CE Elantech, Inc., Lakewood, NJ, USA; Note: any use of trade, firm, or product names is for descriptive purposes only and does not imply endorsement by the U.S. Government.) at the Environmental Measurements Facility (EM1) at Stanford University. To measure the total carbon (TC) of the samples, 20–30 mg of ground soil samples were weighed into tin capsules and loaded into the analyzer. A standard method was used to measure total inorganic carbon (TIC) and total organic carbon (TOC;

Loeppert & Suarez, 1996). Briefly, 400 mg of ground soil sample was added to a scintillation vial. Then 4 ml of 3-M $HCl_{(aq)}$ was slowly added to the vial via a pipette to remove inorganic carbonate, and the vial was capped loosely. The vial was swirled occasionally for 15 min, and the cap was removed to displace accumulated CO_2 until the weight of the vial stopped changing. The solution was centrifuged to remove the supernatant, and the soil pellet was air-dried and ground with agate mortar and pestle, then 20–30 mg of ground soil samples was weighed into tin capsules and injected into the analyzer to measure the remaining TOC. TIC is the difference between TC and TOC (Table 1). Three measurements for both TC and TOC were performed for each sample to test the accuracy and precision of the TC and TOC values (standard deviation shown in Table 1).

Lost on Ignition (LOI) analysis was performed on the soil samples collected at a 10-cm-depth interval. A standard step-heating method was used to measure the amount of TOC and TIC of the samples (Heiri et al., 2001). Approximately 0.5 g of each soil sample was weighed into ceramic crucibles and oven dried under 100 °C for over 12 hr (Thermo Electron LED GmbH, Langenselbold, Germany) to remove any residual water. The oven-dried samples were then heated to 550 °C for 4 hr using a Muffle Furnace (Thermo Scientific Thermolyne Small Benchtop Muffle Furnaces, Asheville, NC, USA). The temperature and duration of this first heating step was chosen to fully remove organic carbon from each soil sample, without decomposing carbonates. The weight of each sample was carefully recorded before heating (weight 1) and upon reaching room temperature after this first heating step (weight 2). After organic carbon removal, all the samples were then heated to 1000 °C for 2 hr to decompose the inorganic carbon (carbonates) in each sample. The weight of each sample was again recorded after they reached room temperature (weight 3). The difference between weights 1 and 2 is reported as a representation of TOC, and the difference between weights 2 and 3 is considered as TIC (Table 1).

Data measured using the EA are converted to TOC assuming that the mass lost is primarily CO_2 and correcting for the mass fraction of carbon in CO_2 (Loeppert & Suarez, 1996). Kumar et al. (2019) suggests a range of 0.257 and 0.278 for converting soil organic matter measured by LOI to TOC for subsurface soil. As such, we chose to use the same factor of 0.273, which lies within the suggested range, to convert soil organic matter to TOC and ensuring a direct comparison between the two methods. As an independent check, we verified that similar TOC values were recovered for the 0- to 50-cm aggregated soil sample from both EA (2.04%) and LOI (1.94%), thus verifying comparison between the two analytical methods.

2.4. Soil Incubations

Incubation vessels were constructed by drilling two holes in the caps of 948-ml glass canning jars. Plastic bulkhead fittings (1/4-inch outer diameter) were installed in the holes with epoxy to prevent gas leakage. Crack-resistant polyethylene tubing (1/4-inch outer diameter and 1/8-inch inner diameter) was connected to both sides of the bulkheads and a plastic one-way valve attached to the external portion of the tubing to seal the chambers. Respiration was then quantified by circulating the headspace in each jar into an LICOR-8100 Infrared Gas Analyzer (Licor Biosciences, Lincoln, NE, USA) and EGM-5 CO_2 Gas Analyzer (PP Systems, Amesbury, MA, USA) to measure CO_2 concentration. During measurements, the upper tube (closest to the cap) was attached to the inlet of the instrument used, and the lower tube (close to the soil) was attached to the outlet to facilitate circulation. Two sets of soil incubation experiments were conducted using two batches of soil samples collected at the site described in section 2.1.

2.4.1. Depth-Averaged Incubations

The first batch was collected in November 2015 and consisted of coarsely aggregated depth intervals (0–52 cm, 63–108 cm, 112–165 cm) as a means of reproducing the aggregate behavior of the soil column under a range of soil moisture contents at a resolution relevant to traditional field observations and large-scale models of overall soil CO_2 flux. For the remainder of the paper, we will refer to data collected from this sample set as the first incubation. Each of the three coarse depth intervals of these soils were divided into four 75-g air-dried subsamples and each of these were subjected to a specified volume of deionized water to produce four distinct *Se* values of 0, 33%, 66%, and 100%. All samples were initially purged with CO_2 free air (zero air, SJ smith) for over 10 times the size of the headspace and kept under 22 °C throughout the experiment. Incubations were run over a 10-day period with daily sampling. After every analysis, the vessels were purged again with CO_2 free air to reset the O_2 and CO_2 concentrations in the headspace. As a result, oxygen limitation to the overall respiration rate is partially mitigated by the

Table 1
Soil Carbon Content of the Two Sets of Soil

	Sample name	Depth	C%	C% stdev	TOC%	TOC% stdev	TIC%	N%	N% stdev	C/N
First incubation	BCM.top.1	0–52	2.64	0.03	2.00	0.41	0.63	0.32	0.00	8.21
	BCM.top.2	0–52	2.54	0.05	2.07	0.32	0.46	0.31	0.01	8.30
	BCM.mid.1	63–108	1.71	0.01	1.44	0.08	0.27	0.23	0.01	7.52
	BCM.mid.2	63–108	1.67	0.06	1.43	0.02	0.23	0.22	0.00	7.67
	BCM.bot.1	112–165	1.04	0.12	0.90	0.02	0.14	0.17	0.01	6.04
	BCM.bot.2	112–165	0.96	0.01	0.89	0.03	0.07	0.17	0.00	5.75
Second incubation	BCT.1	0–10	3.21	—	2.77	—	0.44	—	—	—
	BCT.1.rep	0–10	3.24	—	2.84	—	0.40	—	—	—
	BCT.2	10–20	2.17	—	1.73	—	0.44	—	—	—
	BCT.2.rep	10–20	2.23	—	1.79	—	0.43	—	—	—
	BCT.3	20–30	2.26	—	1.82	—	0.43	—	—	—
	BCT.4	30–40	2.08	—	1.64	—	0.44	—	—	—
	BCT.5	40–50	2.15	—	1.69	—	0.46	—	—	—
	BCT.5.rep	40–50	2.04	—	1.6	—	0.44	—	—	—

replenishment of the headspace; however, high fluid saturation levels in some of the experiments still support oxygen-limited rates. All respiration rates are calculated by measuring the CO_2 accumulated over the prior 24-hr interval and are thus interpreted as the average respiration rate of the previous day (Table 2).

2.4.2. Spatially Resolved Incubations

We note that though these coarsely sampled soils provide an aggregated response, which we utilize as a general representation of the relationship between soil moisture and respiration rate, these data are the integrated behavior of several soil horizons resulting from physical mixing of approximately 50-cm intervals of the soil depth profile. In addition, the choice of a 24-hr sampling interval is coarse compared to many prior incubation methods (Blazewicz et al., 2014; Meisner et al., 2015). Thus, the extent to which these data reflect or obscure shorter timescale responses or differences in behavior as a function of depth is unclear. To explore this behavior and the associated fidelity of our models across multiple spatial and temporal scales, a second set of soil samples were recovered from the same field site in June 2016, consisting of a higher-resolution depth interval (10-cm increments) to a maximum depth of 50 cm. These samples were subjected to the same collection, preservation and preparation procedures as the coarser sample set and used to conduct a second incubation experiment at 66% *Se* using an experimental setup identical to the first incubation. For the remainder of the paper, we will refer to data collected from this sample set as the second incubation. In addition to these high-resolution incubations, we also used the second set of soil samples to recreate the

Table 2
CO_2 Respiration Data From Incubation Experiments

			Cumulated time spend (hr)						
			0	24	48.5	72.5	96	139.5	186.5
	Soil depth (cm)	Moisture content (%)	CO_2 flux (μmol/g soil/day)						
BCM-top-0	0–52	0	0	0.151	0.080	0.064	0.038	0.026	0.028
BCM-top-1		33	0	3.106	2.189	1.689	1.449	1.150	0.902
BCM-top-2		66	0	4.808	5.307	3.222	2.310	1.697	1.317
BCM-top-3		100	0	2.585	2.906	2.662	2.118	1.711	1.563
BCM-mid-0	63–108	0	0	0.309	0.216	0.163	0.101	0.077	0.071
BCM-mid-1		33	0	1.705	1.392	1.116	0.795	0.646	0.562
BCM-mid-2		66	0	2.235	3.188	2.084	1.257	0.909	0.795
BCM-mid-3		100	0	1.181	1.669	1.320	1.034	0.870	0.831
BCM-bot-0	112–165	0	0	0.406	0.253	0.178	0.096	0.063	0.061
BCM-bot-1		33	0	1.279	0.667	0.469	0.258	0.183	0.177
BCM-bot-2		66	0	1.140	0.834	0.664	0.385	0.309	0.296
BCM-bot-3		100	0	0.610	0.553	0.366	0.365	0.318	0.299

Table 3
Parameter Sets for First-Order Models

	FO1	FO2	Description
Parameter			
$k_{sol,1}$ (1/hr)	N/A	5.0×10^{-4}	
$k_{sol,2}$ (1/hr)	5.0×10^{-5}	5.0×10^{-5}	Decomposition rate constant (adjusted from Manzoni et al., 2014)
f_s (unitless)	0.1	0.1	Proportion of carbon used for microbial growth
f_e (unitless)	0.9	0.9	Proportion of carbon used for microbial respiration
$k_{up,1}$ (1/hr)	N/A	4.0×10^{-2}	Microbial uptake rate constant for fast-responding biomass
$k_{up,2}$ (1/hr)	1.53×10^{-2}	2.0×10^{-2}	Microbial uptake rate constant for slow-responding biomass
k_{mor} (1/hr)	4.17×10^{-5}	4.17×10^{-5}	Mortality rate constant for biomass (adjusted from Manzoni et al., 2014)
$Se_{thres,1}$ (unitless)	N/A	25%	Threshold effective saturation
$Se_{thres,2}$ (unitless)	60%	55%	Threshold effective saturation
Initial condition			
Se	Variable	Variable	
C (mass fraction)	0.02	0.02 (upper), 0.014 (middle), 0.009 (lower)	Total carbon fraction (measured)
C_{total} (gC/m^{3}H$_2$O)	$C \times 1518720$	$C \times 1518720$	Total carbon concentration (unit converted from C)
$C_{sub,1}$ (gC/m^{3}H$_2$O)	N/A	$1/4 \times 0.875 \times C_{total}$	Concentration for substration carbon
$C_{sub,2}$ (gC/m^{3}H$_2$O)	$0.877 \times C_{total}$	$3/4 \times 0.88 \times C_{total}$	Concentration for substration carbon
$C_{soluble,1}$ (gC/m^{3}H$_2$O)	N/A	$1/4 \times 0.025 \times C_{total} \pm 20\%$	Concentration for soluble carbon
$C_{soluble,2}$ (gC/m^{3}H$_2$O)	$0.023 \times C_{total} \pm 20\%$	$3/4 \times 0.02 \times C_{total} \pm 20\%$	Concentration for soluble carbon
Bio$_1$ (gC/m^{3}H$_2$O)	N/A	$1/4 \times 0.10 \times C_{total}$	Concentration for fast-responding biomass
Bio$_2$ (gC/m^{3}H$_2$O)	$0.10 \times C_{total}$	$3/4 \times 0.10 \times C_{total}$	Concentration for slow-responding biomass

aggregated 0- to 52-cm incubation conducted in the first sample set by carefully mixing 15 g of each 10-cm depth interval to form a direct comparison. The CO_2 concentration data for this second experiment were collected at higher temporal frequency (1–4 hr) for approximately 3 days as a means of constraining a more detailed time series of soil respiration rate after a wetting event. In total, this second incubation experiment not only serves as a replicate of the aggregated (0–52 cm) sample but further expands accurate representation of the variation in respiration rate across higher depth resolution and over smaller time intervals.

2.5. Model Development

For both models, the initial conditions are constrained by the experimental setup and sample characterization, including the composition of the headspace and content of organic carbon. Several parameters are not directly constrained, such as the proportion of labile and recalcitrant carbon concentrations and the distribution of rapid and slow microbial populations. The starting concentrations of soluble carbon pools in each simulation is approximated based on the EA measurements (Tables 3 and 4) and assuming a water extractable percentage of approximately 1–2% consistent with previous studies (Boyer & Groffman, 1996; Chantigny, 2003). A ±20% variation (80% to 120%) on this value is also included to illustrate sensitivity for all four models considered in this paper (FO1, DM1, FO2, and DM2). Remaining parameters discussed in detail below are constrained by linear regression to the incubation datasets to determine optimal values, and sensitivity tests are included. All parameters are kept consistent between simulations of the incubation datasets over a range of different *Se*. All flux rate and pool concentration units are in gC/m^3-soil/hr, and gC/m^3-soil, respectively.

2.5.1. First-Order Model

In our "first-order" model framework, organic carbon is categorized into three pools: substrate carbon, soluble carbon, and biomass (Figure 2a). Substrate carbon represents a complex carbon form that cannot be directly accessed by microbial communities for respiration. Through a solubilization process, this complex carbon is converted to soluble carbon, which is considered bioavailable for respiration and production of CO_2. The solubilization rate is linearly dependent on the amount of substrate carbon,

$$R_{sol,ij} = k_{sol,i} \times F_{Se,j} \times C_{sub,i} \quad (1)$$

where $R_{sol,ij}$ is the solubilization rate (gC/m^3/hr), $k_{sol,i}$ is the solubilization rate constant (hr^{-1}), and $C_{sub,i}$ is the concentration of the substrate carbon (gC/m^3). We note that the solubilization of substrate carbon is only

Table 4
Parameter Inputs for the Dormancy Models

	DM1	DM2	Description
Parameter			
a (unitless)	20	20	Transition coefficient (Manzoni et al., 2014)
$_{sol,1}$ (1/hr)	N/A	1.16×10^{-4}	Decomposition rate constant (adjusted from Manzoni et al., 2014)
$k_{sol,2}$ (1/hr)	4.17×10^{-5}	1.03×10^{-5}	Decomposition rate constant (adjusted from Manzoni et al., 2014)
f_s (unitless)	0.1	0.1	Proportion of carbon used for microbial growth
f_e (unitless)	0.9	0.9	Proportion of carbon used for microbial respiration
$k_{up,1}$ (1/hr)	N/A	1	Microbial uptake rate constant for fast-responding biomass
$k_{up,2}$ (1/hr)	8	4	Microbial uptake rate constant for slow-responding biomass
$C_{half,1}$ (gC/m^3)	N/A	15,000	Half saturation for soluble carbon
$C_{half,2}$ (gC/m^3)	45,000	45,000	Half saturation for soluble carbon
$k_{tran,1}$ (1/hr)	N/A	1	Transition rate constant between active and dormant biomass for fast-responding biomass
$k_{tran,2}$ (1/hr)	0.017	0.017	Transition rate constant between active and dormant biomass for slow-responding biomass
$Se_{half,1}$ (unitless)	N/A	25%	Half saturation for effective saturation for fast-responding biomass
$Se_{half,2}$ (unitless)	55%	55%	Half saturation for effective saturation for slow-responding biomass
b (unitless)	4.9	4.9	Pore size distribution parameter
$k_{mor\text{-}a}$	4.17×10^{-5}	4.17×10^{-5}	Mortality rate constant (active) (Manzoni et al., 2014)
$k_{mor\text{-}d}$	4.17×10^{-6}	4.17×10^{-6}	Mortality rate constant (dormant) (Manzoni et al., 2014)
Initial condition			
Se	Variable	Variable	
C (mass fraction)	0.02	0.02 (upper), 0.014 (middle), 0.009 (lower)	Total carbon fraction (measured)
C_{total} (gC/m^{3}H$_2$O)	$C \times 1518720$/Se	$C \times 1518720$/Se	Total carbon concentration (unit converted from C)
$C_{sub,1}$ (gC/m^{3}H$_2$O)	N/A	$1/4 \times 0.876 \times C_{total}$	Concentration for substration carbon
$C_{sub,2}$ (gC/m^{3}H$_2$O)	$0.893 \times C_{total}$	$3/4 \times 0.894 \times C_{total}$	Concentration for substration carbon
$C_{soluble,1}$ (gC/m3H$_2$O)	N/A	$1/4 \times 0.024 \times C_{total} \pm 20\%$	Concentration for soluble carbon
$C_{soluble,2}$ (gC/m^{3}H$_2$O)	$0.007 \times C_{total} \pm 20\%$	$3/4 \times 0.006 \times C_{total} \pm 20\%$	Concentration for soluble carbon
Bio$_{active,1}$ (gC/m^{3}H$_2$O)	N/A	0	Concentration for fast-responding active biomass
Bio$_{active,2}$ (gC/m^{3}H$_2$O)	0	0	Concentration for slow-responding active biomass
Bio$_{dormant,1}$ (gC/m^{3}H$_2$O-undiluted)	N/A	$1/4 \times 0.1 \times C_{total} \times$ Se	Concentration for fast-responding dormant biomass
Bio$_{dormant,2}$ (gC/m^{3}H$_2$O-undiluted)	$0.1 \times C_{total} \times$ Se	$3/4 \times 0.1 \times C_{total} \times$ Se	Concentration for slow-responding dormant biomass

one of many factors that may ultimately contribute to the generation of bioavailable carbon, such as carbon transportation and the exposure of physical protection carbon through soil breakdown. As such, this solubilization rate should be considered as a combined effect of all the possible bioavailable carbon input in the current study. $F_{Se,j}$ is a nondimensional factor constraining the solubilization and respiration rates based on Se (equation (2)). The subscript i denotes a given subcategory of the total organic carbon (e.g., allowing consideration of a range of recalcitrance), assuming different forms of substrate carbon will form into consistently different forms of soluble carbon. Similarly, the subscript j denotes different subcategories of microbial organisms that contribute to the solubilization of such substrate carbon.

The behavior of $F_{Se,j}$ is such that a sharp linear increase occurs as a function of Se up to a threshold, $Se_{thres,j}$ followed by a parabolic decrease in respiration for values of Se above the threshold until total saturation is reached (Cabon et al., 1991; Gusman & Mariño, 1999; Porporato et al., 2003):

$$F_{Se,j} = \begin{cases} \dfrac{Se}{Se_{thres,j}}, 0 \le Se < Se_{thres,j} \\ \dfrac{Se_{thres,j}}{Se}, Se_{thres,j} \le Se \le 1 \end{cases} \quad (2)$$

The threshold effective saturation is defined as the value of Se at which the respiration rate reaches its maximum. Different $Se_{thres,j}$ have been applied to uptake pathways simulating the distinct optimal Se for

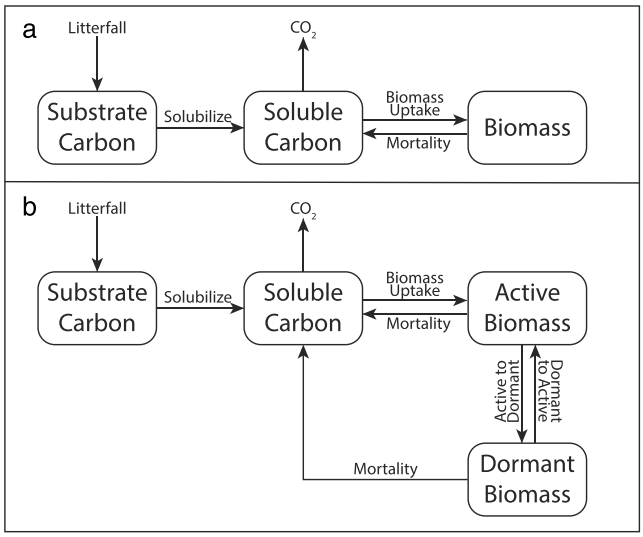


Figure 2. The conceptual models for both (a) first-order, and (b) dormancy (adjusted from Manzoni et al., 2014). Boxes indicate distinct carbon pools, and arrows indicate the reactive pathways of carbon between the pools.

different microbial communities. An arbitrary choice of $Se_{\mathrm{thres},j} = 60\%$ is presented as an illustrative example of the behavior of this factor (Figure S1).

The total microbial respiration rate (i.e., mineralization from soluble carbon to CO_2) is treated as the sum of a series of simple pseudo-first-order kinetic rate expressions with respect to n subcategories of different soluble organic carbon classes,

$$U_{FO} = \sum_{i,j}^{n,m} k_{\mathrm{up},i} \times F_{Se,j} \times C_{\mathrm{soluble},i} \tag{3}$$

where $k_{\mathrm{up},i}$ is the first-order maximum uptake rate constant (hr^{-1}), and $C_{\mathrm{soluble},i}$ is the concentration of soluble carbon belonging to a given compositional subgroup ($\mathrm{gC/m^3}$).

Net respired carbon is a result of two metabolic pathways: catabolic and anabolic. In the catabolic pathway, soluble carbon is converted into CO_2 for energy production, while in the anabolic pathway it is assimilated by the microbes as new biomass, resulting in biomass growth (Lawrence et al., 2009; S. Manzoni et al., 2014). In this first-order model, it is assumed that 90% of respired carbon is converted to CO_2, leaving the remaining 10% for the anabolic growth pathway. Different values should be used in different simulations.

Microbial turnover, including deceased and lysed microbial cells, are treated as a form of soluble carbon and are thus bioavailable (S. Manzoni et al., 2014). The total mortality rate is considered the sum of first-order functions of m subcategories of living biomass (e.g., allowing consideration of a range of response rates and optimal Se values) for different microbial subcategories:

$$RM = \sum_{\mathrm{j}=1}^{m} k_{\mathrm{mor}} \times Bio_j \tag{4}$$

where RM is the amount of biomass that dies in a given time increment ($\mathrm{gC/m^3/hr}$), k_{mor} is the mortality rate constant (hr^{-1}), and Bio_j is the biomass concentration ($\mathrm{gC/m^3}$). For simplicity, we assume that the mortality rate constant is identical for all microbial populations.

Simple mass balance equations are implemented in combination with equations (1)–(4) to account for all inputs and outputs across each carbon pool. For example, the substrate carbon pool is calculated as

$$C_{\mathrm{sub\,new}} = C_{\mathrm{sub\,old}} - R_{\mathrm{sol}} \times \Delta t \tag{5}$$

where Δt is the duration of each time step (hr).

These series of equations were implemented in a commercial software package (Matlab Release 2017a, The MathWorks Inc., Natick, MA, 2016; Note: any use of trade, firm, or product names is for descriptive purposes only and does not imply endorsement by the U.S. Government.). The performances of the first-order model with a single microbial community and category of organic carbon (m, $n = 1$, referred to as FO1), and two microbial communities along with two subcategories of organic carbon (m, $n = 2$, referred to as FO2) are further evaluated in section 3.3.

2.5.2. Dormancy Model

The second model, which we refer to as the "dormancy" model, is modified from the approach of Manzoni et al. (2014) to allow for changes in the biomass in response to changes in effective saturation. Within the dormancy model, the biomass pool is subdivided into two subcategories, active biomass and dormant biomass, with the other two carbon pools remaining the same (Figure 2b), which avoids the uncertainty of an empirical enzyme parameter ($Se_{\mathrm{thres},i}$). By eliminating the empirical factor $F_{Se,j}$, we use a true first-order solubilization rate for the dormancy model, assuming that the solubilization rate is independent of shifts in Se,

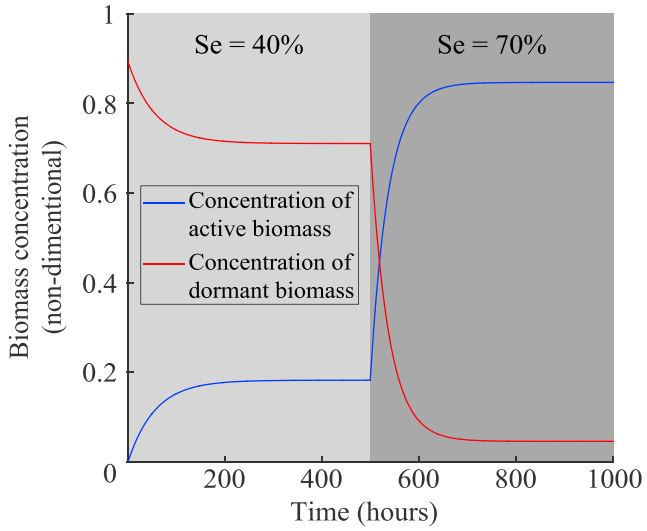


Figure 3. Transition between active and dormant biomass as a function of equations (8) and (9). Starting active and dormant biomass concentrations are set to 0 and 1, respectively. As the simulation begins, an initial Se_{sample} of 40% has been present for a sufficient period of time such that the active and dormant biomass pools are in steady state. At a time t = 500 hr, the Se_{sample} is increased to a new value of 70%, leading to a shift in the distribution of active and dormant biomass.

$$R_{sol,i} = k_{sol,i} \times C_{sub,i} \quad (6)$$

Contrary to equation (1), this approach allows for maintenance of high solubilization rates in dry conditions, resulting in an accumulation of soluble carbon that can be readily decomposed in the next wetting event. Again, we emphasize that this solubilization rate constant should be considered as an effective parameter representing the overall production rate of bioavailable carbon. We note that this calculation of the solubilization rate (equation (6)) is distinct from the first-order model, and thus direct comparison between the two simulations requires careful treatment. We accomplish this in section 3.3 where we directly demonstrate comparable rates obtained from equations (1) and (6) using the FO framework, such that fair comparison between the two models is maintained.

Distinct from the first-order model described in the previous section, the total microbial respiration rate (U_D) is treated here as a dual Monod rate law, which is a function of the amount of active biomass and the availability of both O_2 and soluble carbon, allowing both soluble carbon and O_2 to be the limiting factor in the reaction:

$$U_D = \sum_{i,j}^{n,m} k_{up,j} \times Bio_{active,j} \times \frac{C_{soluble,i}}{\left(C_{soluble,i} + C_{half,i}\right)} \times \frac{O_{2(aq)}}{\left(O_{2(aq)} + K_{half}\right)} \quad (7)$$

where $k_{up,j}$ is the maximum uptake rate constant (hr^{-1}), $Bio_{active,j}$ is the concentration of (active) biomass (gC/m^3), $C_{soluble,i}$ is the concentration of soluble carbon (gC/m^3), and $C_{half,i}$ is the amount of soluble carbon where the uptake rate is 0.5 of the maximum value (also known as the half saturation constant, gC/m^3). The subscripts i and j denote different subcategories of soluble carbon and microbial communities, respectively, similar to the first-order model, and the superscripts n and m denote the quantity of soluble carbon and microbial community subcategories, respectively. The $O_{2(aq)}$ is dissolved oxygen concentration in water (gC/m^3) in equilibrium with a specified partial pressure of O_2 (bar), and K_{half} is the half-saturation constant of the dissolved oxygen concentration (gC/m^3). Similar to the first-order model, 90% of the total respired carbon is converted to CO_2, leaving the remaining 10% as anabolic growth.

In addition, we use a simplified version of the Manzoni et al. (2014) expressions for time-dependent rates of microbial activation and dormancy:

$$Rate_{a\to d,j} = k_{tran,j} \times 1 / \left(1 + \left(\frac{Se_{sample}}{Se_{half,j}}\right)^{b}\right) \times Bio_{active,j} \quad (8)$$

$$Rate_{d\to a,j} = k_{tran,j} \times 1 / \left(a \times \left(\frac{Se_{half,j}}{Se_{sample}}\right)^{b} + 1\right) \times Bio_{dormant,j} \quad (9)$$

where Se_{sample} is the effective saturation of the sample, and the variable $k_{tran,j}$ is the maximum transition rate constant (hr^{-1}), while $Se_{half,j}$ is the saturation at which equation (8) is equal to $0.5 \times k_{tran,j}$. Different $Se_{half,j}$ can be derived from the original form of equations (8) and (9), as in Manzoni et al. (2014), assuming a constant ratio between the two values. Parameter "a" is used in equation (9) to simplify the functional form by using the same $Se_{half,j}$ for both rates. The pore size distribution parameter "b" is adjusted from the Brooks-Corey equation based on a water retention curve (Brooks & Corey, 1964). In this study, the b value employed by Manzoni et al. (2014) is used (Table 4).

This mechanism assumes a time-dependent competition between activation and dormancy as a response to perturbations in effective saturation, which eventually stabilizes to reflect the balance between the two rates such that a dynamic equilibrium between the population of active and dormant biomass is achieved. An example of this behavior is provided in Figure 3. The example illustrates the characteristic response to a wetting event with an assumed rate constant of 1 hr^{-1}. All the other parameters used in this simulation are reported in Table 4.

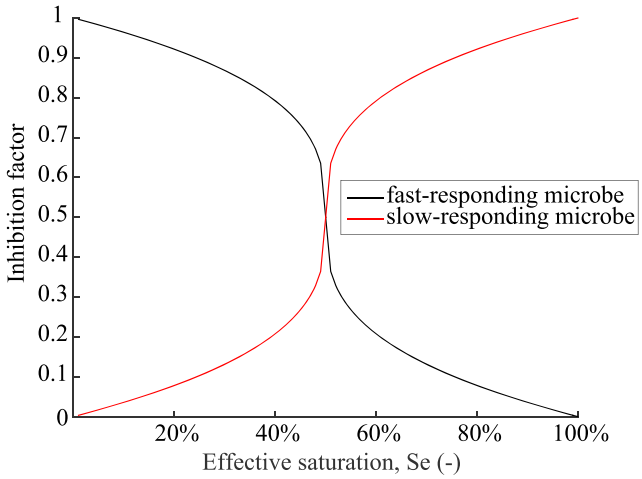


Figure 4. Inhibition factor for both fast- and slow-responding microbial populations as a function of *Se* (equations (10)–(12)). The red line represents the slow-responding population, while the black line represents fast-responders.

In addition, the complexity with which activation rates are treated in the dormancy-based approach requires further consideration of how multiple biomass subcommunities should be implemented. Specifically, if optimal *Se* conditions support the rapid activation of a given microbial population, then it follows that unfavorable *Se* conditions can inhibit a given community (R.L. Barnard et al., 2015; Romain L Barnard et al., 2013). In contrast, such inhibition is vital to dormancy kinetics and should significantly alter the peak height and position of the simulation.

Thus, an additional *Se*-dependent inhibition factor is multiplied in the dual Monod expression which is specific to the two microbial populations:

$$U_{i=\mathrm{lab},j=R} = \mathrm{k}_{\mathrm{up},R} \times Bio_{\mathrm{active},R} \times \frac{C_{\mathrm{sol,lab}}}{\left(C_{\mathrm{sol,lab}} + C_{\mathrm{half,lab}}\right)} \times \frac{O_{2(\mathrm{aq})}}{\left(O_{2(\mathrm{aq})} + K_{\mathrm{half}}\right)} \times \left(\frac{1-\left(2Se_{\mathrm{sample}}-1\right)^{1/3}}{2}\right) \quad (10)$$

$$U_{i=\mathrm{lab},j=T} = k_{\mathrm{up},T} \times Bio_{\mathrm{active},T} \times \frac{C_{\mathrm{sol,lab}}}{\left(C_{\mathrm{sol,lab}} + C_{\mathrm{half,lab}}\right)} \times \frac{O_{2(\mathrm{aq})}}{\left(O_{2(\mathrm{aq})} + K_{\mathrm{half}}\right)} \times \left(\frac{\left(2Se_{\mathrm{sample}}-1\right)^{1/3}+1}{2}\right) \quad (11)$$

$$U_{i=\mathrm{rec},j=T} = k_{\mathrm{up},T} \times Bio_{\mathrm{active},T} \times \frac{C_{\mathrm{sol,rec}}}{\left(C_{\mathrm{sol,rec}} + C_{\mathrm{half,rec}}\right)} \times \frac{O_{2(\mathrm{aq})}}{\left(O_{2(\mathrm{aq})} + K_{\mathrm{half}}\right)} \times \left(\frac{\left(2Se_{sample}-1\right)^{1/3}+1}{2}\right) \quad (12)$$

where $k_{\mathrm{up},r}$ and $k_{\mathrm{up},K}$ are maximum uptake rate constants (hr^{-1}) specific to the $Bio_{\mathrm{active},R}$ and $Bio_{\mathrm{active},T}$ subpopulations, respectively (Table 4).

This form of inhibition factor provides valid numbers across the full range of *Se* values with a value of 1 when $Se = 100\%$ and 0 when $Se = 0$ for T group biomass, thus limiting the respiration rates at lower *Se* values with a gradient at intermediate values. Meanwhile, the opposite behavior is specified for the R group biomass limiting their respiration capability at higher *Se* values (Figure 4).

Microbial mortality is treated in the same manner used in the first-order model (equation (4)), with distinct mortality rate constants assigned for active and dormant biomass (referred to as $k_{\mathrm{mor}-a}$ for active biomass, and $k_{\mathrm{mor}-d}$ for dormant biomass). The mortality rate of dormant biomass is set 10-fold lower than that of the active biomass in this study. In addition, the mass balance calculation is treated in a similar manner as the first-order model.

As with the first-order model described previously, the performance of the dormancy model with a single microbial community and category of organic carbon (m, $n = 1$, referred to as DM1), and two microbial

communities along with two subcategories of organic carbon (m, $n = 2$, referred to as DM2) are further evaluated in section 3.3.

2.6. The AIC

The Akaike Information Criterion (referred to as AIC; Akaike, 1998) is used to quantitatively score the two models with the consideration of both the precision of the simulation and the number of parameters used. The Residual Sum of Squares (RSS), a parameter that quantitatively evaluates the goodness of fit, is first calculated,

$$RSS = \sum_{k=1}^{n} (MO_k - In_k)^2 \tag{13}$$

where MO_k is the model output and In_k is the incubation data. The subscript k denotes different data points in a given depth and Se, and the superscript n represents the total quantity of data points.

While RSS values illustrate the goodness of fit, the number of parameters is included in the AIC calculation as

$$AIC = n \log(RSS/n) + 2l \tag{14}$$

where l represent the number of parameters. Thus, a better overall model performance is achieved with a lower AIC value which encapsulates both the ability to reproduce the observed data and the number of parameters necessary to do so.

2.7. Model Calibration

All model parameter calibration was systematically conducted using the following procedure:

1. First, we minimized the number of free parameters. Specifically, we fixed parameters Se_{thres} and k_{mor} for the FO model, as well as parameters a, b, and Se_{half} for the DM model using appropriate values from previous studies (Howard & Howard, 1993; Linn & Doran, 1984; Manzoni et al., 2014) and setting the initial carbon mass fraction to values measured using the EA or LOI.
2. Next, we fixed f_s, f_e, and k_{up} for both FO and DM models, as well as k_{tran} and C_{half} for the DM model, using parameter values in agreement with previous studies (Bowen & Beerling, 2004; Manzoni et al., 2014).
3. We then use an Optimization Toolbox (Matlab Release 2017a, The MathWorks Inc., Natick, MA, 2016; Note: any use of trade, firm, or product names is for descriptive purposes only and does not imply endorsement by the U.S. Government.) to systematically adjust k_{sol} and the initial fraction of soluble carbon for both FO and DM models to values that ensure the lowest RSS. Optimization was run for 1,000 randomly selected parameter combinations for both FO and DM models from a range of k_{sol} values between 10^{-10} and 10^{0} hr^{-1}, and a range of initial soluble carbon concentrations between 0 and 0.2 $\text{gC/m}^3\text{H}_2\text{O}$. Each of these parameter sets serves as an initial guess, from which the optimization algorithm reaches updated values that achieve a minimum RSS. This Monte Carlo method allows us to verify that we have reached a global minima (code available on a GitHub repository described in the Acknowledgments section). Critically, once our Monte-Carlo-optimized parameter set is obtained, all of these values are kept identical in each model (FO1, FO2, DM1, and DM2) for all simulations across the entire range of soil depths. The only two parameters that change are Se (representing the range of soil moisture values used in the experiments) and the initial carbon mass fraction (representing the soil depths as constrained by direction measurements; section 2.3). All model parameters were then varied ±10% as a sensitivity test. Results are reported as percentage higher than minimum residual sum of squares (Table S2) and further discussed in section 4.2.

3. Results

3.1. Soil Measurements and Incubation Results

The concentrations of TOC in each depth of the two sets of soil samples are given in Table 1. The results show that TOC decreases with depth for both sets, which is expected as organic inputs associated with biological activity are most abundant at the surface and decline with depth. In addition, the TIC also decreases with depth for the coarse samples, suggesting that the highest carbonate concentration occurs at a depth

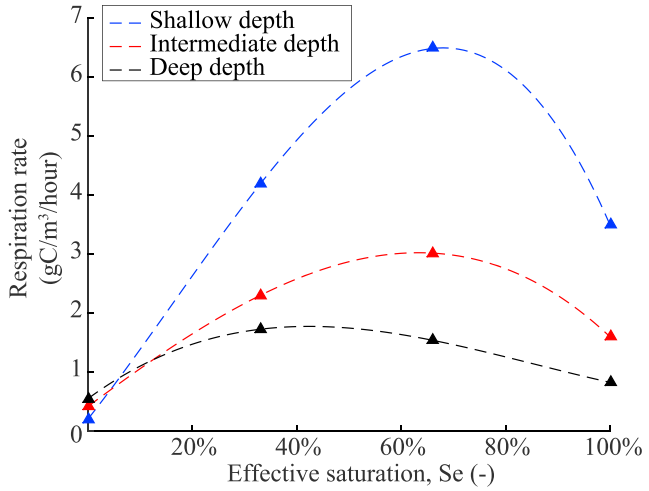


Figure 5. Respiration rate as a function of four values of *Se* (filled triangles) fitted with dashed lines to illustrate trends. Measurement uncertainties lie within symbols (<1.5% of the measured concentration). Soil respiration rates are shown for the first 24 hr of incubation for all three soil depths (0–52 cm (blue), 63–108 cm (red), and 112–165 cm (black)) at different effective saturations (*Se* = 0, 33%, 66% and 100%).

shallower than 52 cm at this sampling site. The TIC of the high-resolution profile does not change significantly, indicating no obvious variation in inorganic carbon content over the top 50 cm. The total nitrogen concentrations for the coarse samples are also given in Table 1, indicating a C/N which decreases slightly with depth from a maximum value of 8.3. We may thus reasonably assume negligible N limitation on microbial growth.

Respiration rates of the first incubation for all three soil depths at different effective saturations (*Se* = 0, 33%, 66%, and 100%) for the first day of incubation show similar patterns across all depths (Figure 5 and Table 2), where respiration rates are positively correlated with effective saturation in dry conditions and negatively correlated in wet conditions. We note that though we purged the headspace of the incubation vessel with CO_2 free air after each measurement to replenish O_2 concentrations to atmospheric level, oxygen limitation could still possibly exist for the samples near fully saturated conditions due to pore wet-up and blockage (as suggested by the drop in respiration rate at high effective saturation). The peak respiration rate for both the shallow and intermediate depths lies around 66% *Se*, while the deepest depth displays a slight shift in maximum value toward 33% *Se*.

Respiration rates evolve with time in all sampled depth intervals for both the first coarse (Figure 6) and second high-resolution (Figure 7) incubation experiments. All respiration rates increase to a maximum value before decreasing to an apparent steady state, as is typical of the Birch Effect. The time to reach peak respiration rate differs across the range of effective saturations tested. For the first incubation experiment, at lower effective saturation (0% and 33%), the peak values appear approximately 24 hr after initiation of the incubation, while at higher moisture content (66% and 100%), this occurs approximately 48 hr after rewetting. Reproducibility of these respiration data was demonstrated using the second incubation experiment in multiple ways. A direct test was included, using two replicates run for splits of the same soil collected from the 20- to 30-cm depth interval (Figure 7a).

The results of the second incubation show unique behavior in the 0- to 10-cm depth interval, which exhibits a rapid rise in CO_2 within the first few hours following rewetting. This large peak in respiration rate reaches a maximum after 5 hr, and subsequently decreases to a quasi-equilibrium thereafter. In contrast, a lagged respiration peak was observed in all deeper sample intervals, reaching a peak at approximately the end of the second day, similar to the behavior of the coarse 0- to 52-cm depth interval in the first incubation. In addition, the averaged respiration rates of the five depths show close resemblance in comparison to the 0–50 cm physically aggregated sample

Notably, this second incubation experiment grants us a unique opportunity to explore the effect of averaging respiration rate in both depth and time. Thus, we further tested the reproducibility and scaling of these data by comparing the integrated respiration rate of the weighted average of the five soil depths at the end of the first, second, and third days to the prior incubation results (Figure 7b). The integrated dataset show close agreement to the previous coarser dataset, indicating that the respiration data acquired from the first incubation experiment is an accurate and robust aggregation of the behavior observed over higher depth and time resolution. However, this averaged respiration rate shows a faster time to reach its peak value after rewetting compared to the previous coarse dataset, which results from the impact of the unique rapid respiration peak noted for the shallowest soil sample collected from 0–10 cm in the depth profile. Such a distinct response sheds valuable insight into the behavior lost when sampling and simulating datasets over coarser depth and time resolutions. This distinction is further discussed in section 4.3.

3.2. Model Results and Evaluation

In order to arrive at an optimal balance between model parameterization and accuracy across the range of sample frequency, and depth resolution data obtained in our incubations, we first evaluate a range of

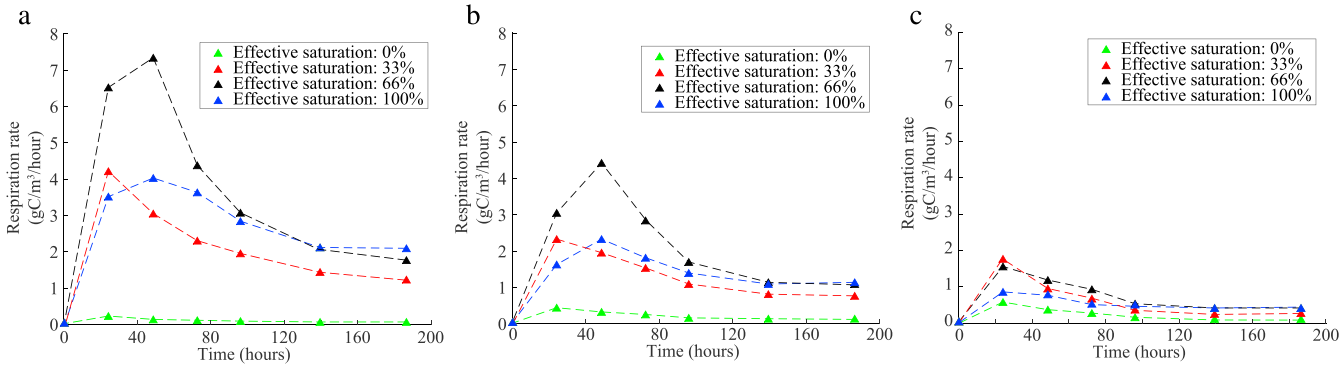


Figure 6. Respiration rate for (a) shallow soil sample (0–52 cm); (b) intermediate soil samples (63–108 cm); (c) deep soil samples (112–165 cm), as a function of time for four values of Se (filled triangles) connected with dashed lines to illustrate trends. Measurement uncertainties lie within symbols (<1.5% of the measured concentration).

model complexity. Specifically, we first focus on the generic trend of the Birch effect recovered by our coarse depth and time resolution samples, as this behavior broadly represents the trends observed for the response of soil respiration to changes in soil moisture with time across a variety of field systems. Thus, we consider an integrated response in our aggregated sample as an instructive dataset to begin our comparison of simulated changes in respiration rate after wetting events. We then expand this model evaluation to the higher spatial and temporal resolution datasets, such that we may draw comparison between the model performance and parameterization across a range of relevant sample resolutions.

The FO1 model was applied to the first incubation experimental results, where the time series data for 66% and 33% *Se* from the shallow soil depth were used as a base case (Figure 8a). The results show reasonable agreement with the data; however, in this simplified approach the model respiration rate decreases monotonically with time (parameter values shown in Table 3).

Since two distinct equations were used to calculate solubilization rate in FO and DM models (equations (1) and (6), respectively), here, we applied both equations to the FO1 model, and performed a direct comparison of these two versions (Figure 8a). The result shows that the respiration rate for the lower *Se* exceeds that for the high *Se* after approximately 85 hr with application of equation (6), which contradicts the data. In addition, we observe that the use of this expression does not influence the monotonic nature of the respiration

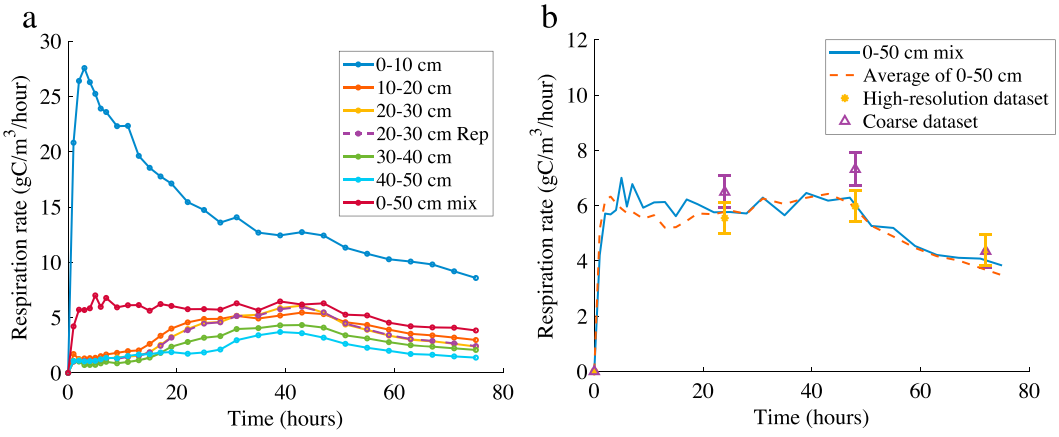


Figure 7. Respiration rates as a function of time for the high-resolution incubation dataset with 10-cm depth increments of soils collected from the East River field site and 1–4 hr sampling interval. (a) The range of soil sampling depths distinguished by color including a replicate of the 20–30 cm interval (dashed line). (b) A comparison between incubation experiments using a sample aggregated over the upper 50 cm (blue line), a weighted average of the higher-resolution 10-cm sample intervals (dashed red line), a 24-hr average of the higher-resolution data (yellow dot), and the coarse sample values collected from an aggregated depth interval of 0–50 cm over a 24-hr sampling interval (purple triangle). The error bars represent ±10% of the measured respiration rate.

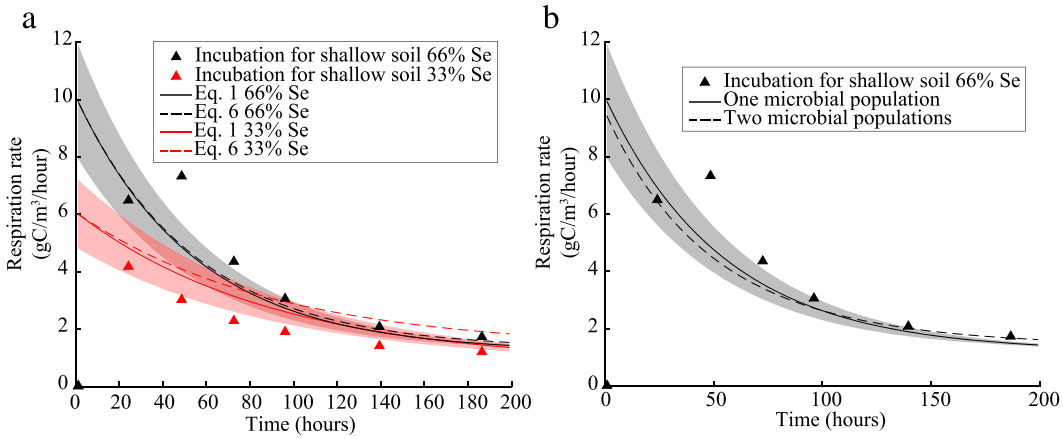


Figure 8. The first-order kinetic model using (a) FO1; solid lines represent model that uses moisture-dependent solubilization law (equation (1)), and dashed lines represent model that uses moisture-independent solubilization law (equation (6)); (b) FO1 (solid line) and FO2 (dashed line) microbial populations (all parameters shown in Table 3). Shaded areas represent range of model output with the initial soluble carbon concentration varied by 20%.

rate as a function of carbon availability. Thus, we conclude that equation (1) is superior for the first-order model, and we use it throughout the remainder of the paper.

Due to the more complex mechanism used in the DM model, the sensitivity of DM1 under a range of $Se_{\mathrm{half},j}$ and $k_{\mathrm{up},j}$ values is illustrated in Figure 9 prior to any simulation (Table 4, Se_{sample} set to 70%). Here, a lower $Se_{\mathrm{half},j}$ value results in faster activation of dormant biomass (equation (9)) and slower dormancy of active biomass (equation (8)), while a larger $k_{\mathrm{up},j}$ value induces more CO_2 produced in one time step (higher peak value) leaving less available soluble carbon in the system. Accordingly, a lower $Se_{\mathrm{half},j}$ and larger $k_{\mathrm{up},j}$ result in a more rapid increase in the respiration rate following rewetting, illustrated by an earlier time of peak CO_2 production with a higher peak value, leaving less available soluble carbon in the system, and thus an earlier decrease to steady state rates. Though the model sensitivity to the $Se_{\mathrm{half},j}$ and $k_{\mathrm{up},j}$ parameters are comparable, we note that the $Se_{\mathrm{half},j}$ parameter alters the point of dynamic equilibrium between the active and dormant biomass, while $k_{\mathrm{up},j}$ changes the rate of microbial uptake regardless of the balance between the two biomass forms.

DM1 was similarly evaluated against the incubation results for 66% and 33% *Se* as a base case (Figure 10). We observed a significant improvement in the ability of this model to represent transient changes in CO_2 respiration rate associated with the rewetting event at early time for 66% *Se* with comparable parameter

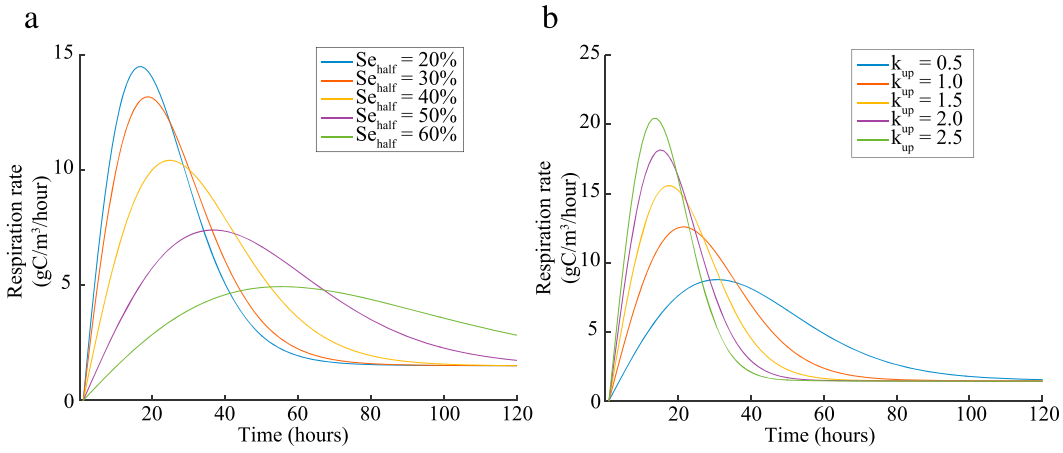


Figure 9. (a) Model sensitivity to a range of Se_{half} values, with all other parameters held constant (Table 4). Different colors represent different Sehalf. (b) Model sensitivity to a range of k_{up} values, with other conditions similar to (a).

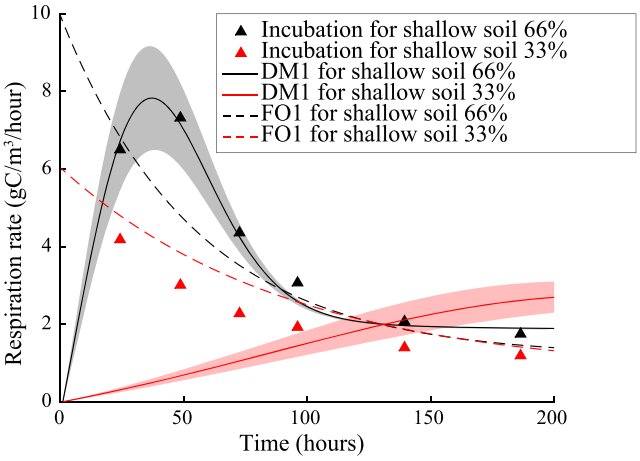


Figure 10. Comparison of model and measured respiration rates for the shallow soil 33% and 66% *Se* values as a function of time. Filled triangles represent experimental data, and lines illustrate output from DM1. Shaded areas represent range of model output with the initial soluble carbon concentration varied by 20%. FO1 outputs (dashed lines) are also plotted here for comparison.

values (Table 4). However, we found the same parameter set is unable to reproduce comparable results for 33% *Se*. In particular, the model results in a slower activation of dormant biomass, which retards the time to peak respiration in comparison to the measured data. This time discrepancy persists regardless of the choice of parameter sets. Thus, we next test a more complex modeling scheme, which features two organic carbon and two microbial pools (DM2).

To improve upon the base case scenario during the transient period following a rewetting event, FO2 and DM2 were tested in a manner similar to the procedure described for FO1 and DM1. Two distinct microbial populations ($m = 2$) were assumed to exist in the soil samples. One of them is capable of activating rapidly after rewetting (indicated as the R group), and the other is characterized by a slower transient activation period (indicated as the T group). In addition, the substrate and soluble organic carbon pools were also subcategorized into labile and recalcitrant subcomponents such that the labile soluble pool is generated by labile substrate carbon and the recalcitrant soluble carbon is produced by recalcitrant substrate carbon. The models were parameterized such that the R group microbial category is more adaptable to dynamic environments. This includes a faster activation rate at lower *Se* and a higher mineralization rate constant for labile organic carbon; however, these R group microbes were assumed to have negligible capacity to mineralize recalcitrant carbon. In contrast, the T group microbial subcategory is characterized by a slower response time with the capacity to utilize both labile and recalcitrant carbon. These differences in rate between the two microbial pools were achieved in the model by variations in $k_{sol,i}$ (equations (1) and (6)), $Se_{thres,j}$ (equation (2)), $k_{up,i}$ (equation (3)), and $k_{up,j}$ (equation (7)). Parameters are shown in Tables 3 and 4.

Results show that despite this additional complexity, the model performance for FO2 was not improved compared to FO1 (Figure 8b). A similar inhibition factor (equations (10)–(12)) was applied to FO2. However, this inhibition linearly reduces the respiration rates of two microbial communities that both feature monotonic variations. As such, the summed respiration rate still shows a monotonic trend that is induced by the first-order kinetics and thus does not improve performance. Based on these results, we conclude that the monotonic trend in CO_2 respiration rate produced by such a first-order approach is largely unaffected by both the extent to which the carbon pools are subdivided into a range of reactivity and the extent to which the microbial communities are subdivided in terms of both carbon utilization efficiency and moisture-dependent activation rate. Thus, FO1 is considered more efficient for the first-order approach, and is utilized throughout this paper as a comparison to the dormancy model.

Similarly, we tested the ability of DM2 to reproduce the respiration datasets corresponding to multiple *Se* values for a common soil sample after calibration (Figure 11a). Incubation results for 100% *Se* were absent in this simulation since our modeling approach included a constant O_2 concentration, which contradicts the experimental condition where O_2 is limited in the pore space at 100% *Se*. DM2 shows clear improvement in simulating soil respiration data with a single parameter set (Table 4) across a range of *Se*. Both shallow and intermediate depth soil sample results are accurately reproduced by the model (Figures 11b and 11c and Table 4), where the only difference in parameter values differentiating the two sets of simulations is the amount of starting substrate carbon based on the EA results (Table 1). The model somewhat overpredicts the respiration rate of deep soil samples. This may result from (1) chronic oxygen limitation at these depths (112–165 cm) in the field, that leads to a distinct microbial community less responsive to moisture fluctuations; (2) physically more protected soil organic carbon at depth, resulting in slower observed respiration rates even under the disruption of an incubation experiment (Rumpel & Kögel-Knabner, 2011).

3.3. Reoptimization at Higher Sample Resolution

Thus far we have described model development and constraints using one (coarse) component of our total incubation dataset. To expand the range of temporal and spatial scales tested with our model, we employed the second, higher resolution (10-cm depth interval, 1- to 4-hr sampling frequency) dataset as a means of

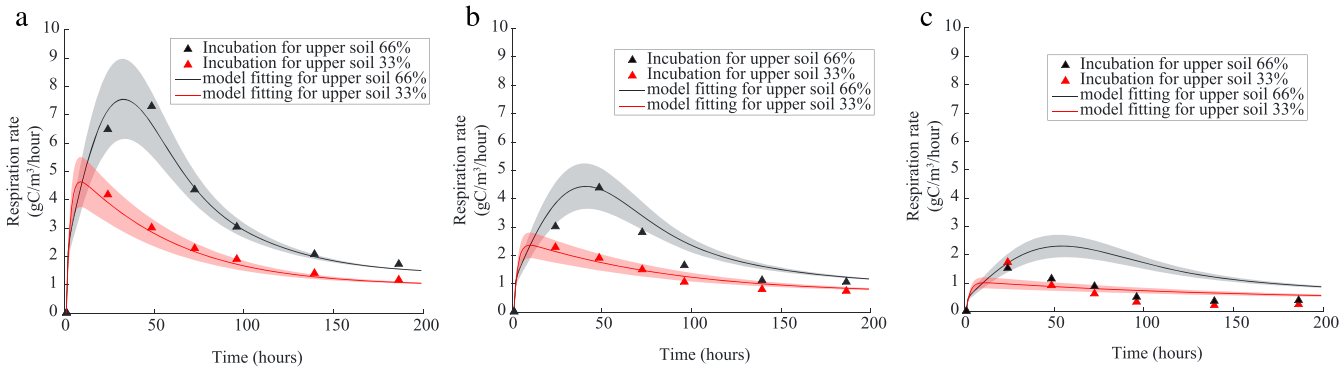


Figure 11. The performance of DM2 when simulating (a) upper soil; (b) middle soil; (c) lower soil at both 33% and 66% *Se*. Shaded areas represent range of model output with the initial soluble carbon concentration varied by 20%.

testing our models across scale and exploring the conditions and reproducibility of the first experiment. Though this high-resolution dataset generally shows close agreement to the coarse data obtained from the first experiment as described in section 3.1 (Figure 7), one notable difference between them is the influence of the 0- to 10-cm respiration rate, which reached a large peak value within 5 hr after rewetting. This behavior was in sharp contrast to the remainder of the soil depth intervals tested and causes both the physically aggregated 0- to 50-cm sample and the average respiration rate of the top 50 cm to rise up to high respiration rates faster than what would be inferred from the coarse 24-hr sample frequency data. In contrast, the rest of the four depth intervals (10–20, 20–30, 30–40, and 40–50 cm) show comparable behavior consistent with the coarse data, including similar timing of peak respiration. As such, we reorganized the dataset in three subsets to accomplish this model comparison across scales: (1) the respiration rate of the 0- to 10-cm depth interval; (2) the average respiration rate of the 10- to 50-cm interval; and (3) the average respiration rate of the 0-to 50-cm interval (Table S3).

To evaluate the capacity of the FO1 and DM2 models to describe our higher resolution and resampled datasets, we reran our simulations using the total organic carbon content of the five shallow 10-cm soil depth intervals (Table 1) as initial conditions. We then reoptimized the parameter values to simulate the three subsets described above (Figure 12). A similar parameter calibration procedure was performed (described in section 3.2). Distinct k_{sol} and k_{up} values were used for the three subsets in order to optimize model simulations for the early peak respiration rate that is shown for the 0- to 10-cm depth interval. These values are further discussed in section 4.3. The results of the DM2 model produce a distinct timing of peak respiration following rewetting as shown in the incubation experiment. In addition, though the performance of FO1 is comparable to DM2 when simulating the 0- to 10-cm depth interval, it fails to demonstrate changes in the timing of peak respiration as a result of the first-order formulation forcing a monotonic decrease from the initial condition. This inability is clearly exposed when simulating the 10- to 50-cm interval, where the Birch-type behavior shows the greatest lag after rewetting. To directly compare the performance of the two models with the consideration of the number of parameters used, the AIC values of these simulations were recalculated (discussed in section 4.3).

4. Discussion

4.1. Capturing the Birch Effect

As is shown in Figure 8, the respiration rate simulated by the simplified approach used in the FO model has a monotonic nature. We note that Oikawa et al. (2014) has successfully simulated such a transient pulse of respiration rate after rewetting using a modified first-order approach, in which a Dual Arrhenius Michaelis-Menten equation was implemented and moderated by the assumption that little soluble carbon exists at the beginning of the wetting event. As a result, their model initially predicts a low respiration rate due to the lack of labile carbon, which they then rapidly increase over the first 48 hr of their simulation in order to drive the appearance of a pulse. In contrast, to the Oikawa et al. (2014) approach, our model

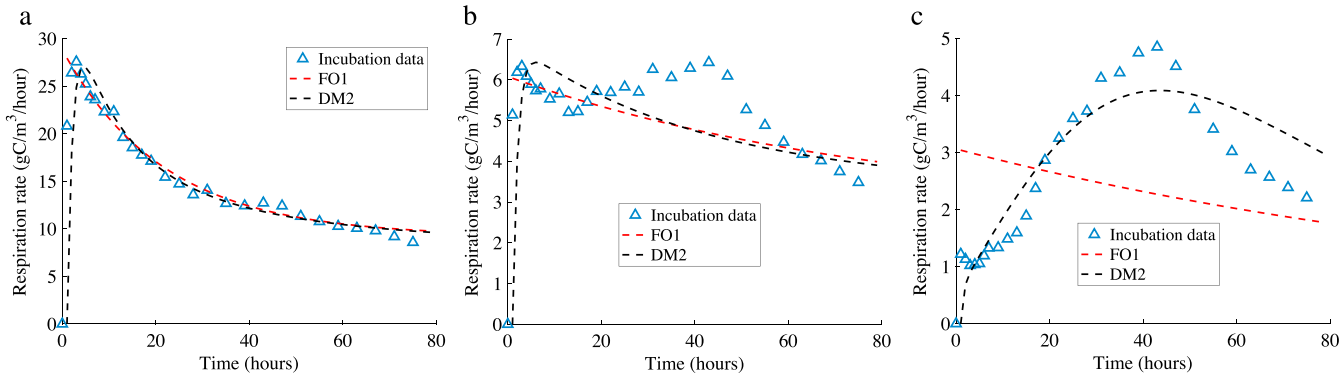


Figure 12. The performance of the FO1 and DM2 models while simulating: (a) 0- to 10-cm depth interval; (b) 0- to 50-cm depth interval; (c) 10- to 50-cm depth interval.

avoids the assumption that extracellular enzymes are inactive in dry conditions, providing compatibility with the inferred buildup of labile carbon during dry periods suggested in prior studies (e.g., Geisseler et al., 2011; Lawrence et al., 2009). In general, modifications of this type to the basic FO model framework produce more accurate representation of simulated pulse responses. Here, we choose to use a basic FO framework as the simplest point of comparison against our proposed dormancy model. Our intent here is not to knowingly create a model structure with obvious limitations to contrast against, but to test the situations in which this widely applied FO framework is suitable and when a more complex model structure is warranted. As such, we already know that the FO model we present here is not capable of accurately representing the transient increase in respiration rate initially observed following a rewetting event (i.e., the Birch effect), but the extent to which this simplification results in a quantitative loss of accuracy in simulating the overall respiration pulse, relative to the cost of additional parameters in our dormancy model, requires constraint.

In contrast, the DM2 model shows a rapid rise at the beginning of the simulation, with a decrease to an equilibrium value through time. This feature is produced by the time-dependent transition between the active and dormant biomass (equation (8) and (9)). At the beginning of each simulation, the transition of the biomass from an initially fully dormant state to predominantly active was triggered by the instantaneous increase in *Se* from 0 to a certain value. This lagged response in respiration rate following an instantaneous rewetting successfully simulated the experimental data. With further time, the excess soluble carbon initially available is depleted, resulting in a decrease of the initially rapid rate of CO_2 production. Ultimately, the rate of soluble carbon consumption (equations (10)–(12)) decreases to a value which is balanced by the rate of substrate carbon solubilization (equation (6)) as the system approaches a steady state. We note that this solubilization rate is an effective value in the current model, which represents many factors that may ultimately contribute to the steady state respiration in natural systems, such as transport limitation and physical protection. For example, in the current framework, oxygen concentration was treated as a constant rather than a limiting factor, assuming that the periodic replenishment of O_2 implemented in our incubation experiments was sufficient for both 33% and 66% *Se* to compensate for consumption due to aerobic respiration.

A key inference demonstrated by the present model results is the need for a quantitative measurement of active vs. dormant vs. dead biomass, which would be needed in order to reliably parameterize either DM1 and DM2 model for a specific soil profile or environmental condition. In the scope of this paper, the intent is not to apply the models to such a specific location or dataset, but rather to demonstrate their relative fidelity against typical Birch-style behavior. As such, by applying a generic parameter set within the DM2 to capture the transition between active and dormant biomass under changing soil moisture, we are better able to represent the Birch behavior with a reasonable initial condition. It is not surprising that DM2 is capable of generating more accurate results than FO1 with the extra flexibility provided by the additional parameters. The extent to which this improved accuracy is offset by the cost of these additional parameters is further considered in a subsequent section (section 4.2).

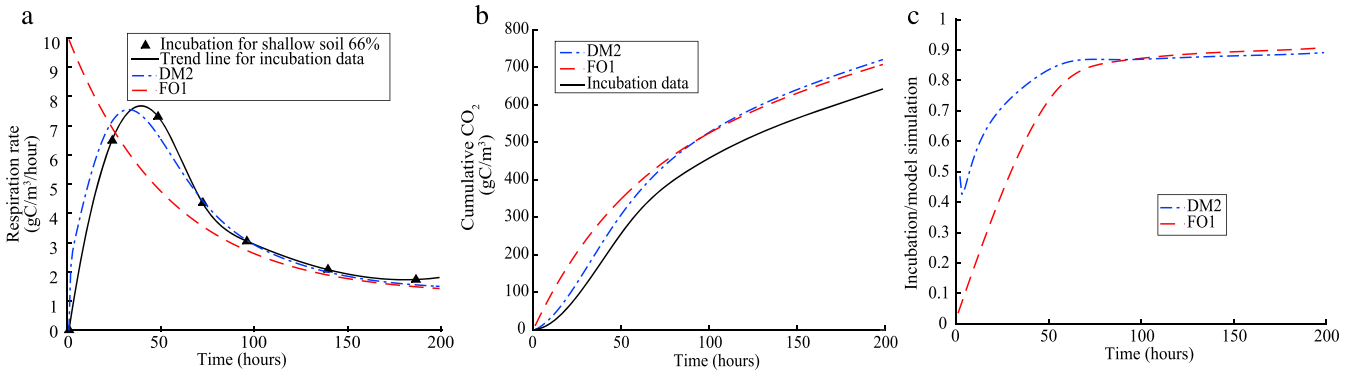


Figure 13. (a) Model output from FO1 and DM2 plotted against incubation data in time series. Measurement uncertainties lie within symbols (<1.5% of the measured concentration). Parameter values for two models are listed in Tables 3 and 4; (b) Cumulative CO_2 concentration integrated from model output and trend line shown in (a); (c) Ratio of integrated incubation data/model output shown in (b) for two models. The dormancy model is clearly a better simulation compared to first-order model within 100 hr (closer to 1).

4.2. Model Precision Versus Cost

Cubic interpolation was used to estimate the rate between incubation data points, allowing us to integrate both the model output and incubation data through time (Figure 13a). The resulting cumulative CO_2 as a function of time estimated by both FO1 and DM2 was then compared against incubation data (Figure 13b) to quantitatively assess the accuracy of each simulation. Even though both models overpredicted the cumulative CO_2 concentration, we observed that FO1 showed a relatively larger overprediction of the amount of CO_2 produced during the initial 50–75 hr of the wetting event. This relatively large overprediction by the first-order model was due to the disparity between the predicted high respiration rate resulting from the monotonic drop and the low respiration rate observed at early time. In comparison, DM2 showed much better agreement to the data for the first ~100 hr, illustrating a better performance with variable *Se*. The ratio of integrated CO_2 concentration between the incubation data and outputs from the two models illustrate the relative performance of the two approaches (Figure 13c). Since the interpolated rates from incubation experiments are consistently lower than outputs from both models (Figure 13b), the ratio of incubation/model CO_2 values fall between 0 and 1 (Figure 13c), where lower values indicate poorer agreement with the experimental data, and 1 indicates an exact match. This exercise demonstrates that the ratio of FO1 is consistently lower than that of DM2 for all times less than 100 hr, indicating that the first-order model cannot accurately simulate the transient changes in respiration rate after soil is rewet (i.e., the Birch effect). After ~100 hr, both models establish close agreement to the data (ratio of integrated CO_2 ~0.9), meaning they are equally accurate at steady state respiration. Thus, in general, the dormancy modeling approach is necessary for accurate representation of dynamic responses to changing *Se* over short time scales, such as in our incubation experiments, with the implementation of a dynamic biomass activation process.

However, we recognize that additional parameterization increases the accuracy of a model at the expense of both computational efficiency and parameter constraint. Thus, the AIC was applied to score the two models. The AIC value of the two models are listed in Table 5.

The results of these model-data comparisons show that the dormancy model not only achieves higher accuracy while simulating the Birch effect but obtains a lower AIC value with soils above the 108-cm depth interval, indicating that this improvement outweighs the extra cost and uncertainty accompanied by the increased model complexity. In contrast, the performance of the first-order model appears superior according to its AIC value in simulating the deepest soils at 66% *Se*. Thus, in the scope of our study, we conclude that DM2 will serve as a better tool in predicting the CO_2 flux of shallow soils subject to frequent moisture fluctuations where the majority of rapid carbon cycling occurs. Moreover, recent studies have demonstrated that Birch effects of this nature can last over the duration of weeks to months and in some ecosystems they may produce over 50% of the total respired CO_2 (Fan et al., 2015). Such inability to capture this Birch dynamic in the first-order framework may generate even larger errors under environmentally relevant

Table 5
AIC Values of the Two Models

		First-order model	Dormancy model
First incubation	Shallow-66%Se	31.0	19.8
	Shallow-33%Se	24.3	6.8
	Intermediate-66%Se	26.3	27.8
	Intermediate-33%Se	20.1	14.4
	Deep-66%Se	21.6	34.8
	Deep-33%Se	15.4	23.9
Second incubation	0–10 cm - 66%Se	115.7	27.8
	10–50 cm ave - 66%Se	44.2	1.8
	0–50 cm ave - 66%Se	31.8	13.8

conditions, indicating that application of DM2 is cost effective and necessary in simulating environments where Birch effects are essential, especially where long periodicity is expected.

However, we also note that the deep-soil component of this sample set, which corresponds to ~13% of the total respiration taken over the shallow, middle, and deep depths, is representative of deep soil carbon storage constituting a significant terrestrial organic carbon stock across a broad diversity of environments. This in turn represents a potentially significant source of atmospheric CO_2 if such carbon were to become mobilized or otherwise biologically available (e.g., disturbances; Trumbore, 2009). Previous studies have employed a diversity of methods, including radiocarbon dating (^{14}C), near-edge X-ray absorption fine structure spectrometry, and differential scanning calorimetry, to explore the chemical properties and stabilization pathways of deep-soil organic carbon (Kleber et al., 2011). However, detailed modeling approaches predicting the behavior of the deep-soil organic carbon are sparse. The results of this model comparison suggest that respiration of deep-soil carbon in our samples is appropriately modeled with a simplified first-order rate law rather than the dormancy rate law. We note that this conclusion is based on an incubation experiment in which we exposed the deep soil samples to an oxygen rich environment analogous to the land surface and thus requires further exploration under in situ conditions. Nonetheless, this finding provides evidence that simplified modeling frameworks are suitable and may be the most appropriate representations of carbon respiration in systems that are not subject to rapid moisture fluctuations. This difference may be related to more stable, high moisture in situ conditions, resulting in a dominant microbial community with low sensitivity to moisture variation.

In addition, model sensitivity analyses show that the microbial uptake rate of the recalcitrant carbon pool ($k_{up,2}$) is particularly important to accurately constrain, exerting approximately 4 times greater influence on the DM2 simulation compared to that of the labile carbon pool ($k_{up,1}$, Table S2). This result suggests, somewhat counterintuitively, that an accurate estimation of the residence time of recalcitrant carbon is vital in order to improve the performance of DM2. In addition, the initial labile carbon concentration has a significant impact on the RSS of the simulation result for DM2. Thus, a direct measurement of the soil labile carbon concentration is recommended in future applications.

4.3. Scaling Between Sampling Resolutions

As is shown in section 3.1, the respiration rates of the second incubation experiment aggregated over the previous 24 hr for the first, second, and third days show close agreement with the 0- to 52-cm data acquired over 24-hr sample intervals in the first incubation experiment (Figure 7). However, the respiration rate of the 0- to 10-cm soil sample reaches a peak value within 5 hr, which is unique to the remainder of the soil depth intervals. When aggregated over the upper 50 cm, this sharp rise is dampened by the delayed response of the rest of the four depth intervals (10–50 cm), yet individually it contributes up to 85% of the overall respired CO_2 of the 50-cm soil column within the first 5 hr after rewetting. This effect drives the magnitude of peak respiration rate averaged over the top 50 cm within the first 5 hr. As time proceeds, the respiration rates of the deeper 10- to 50-cm intervals begin to increase, reaching their peak values at approximately 48 hr. Over this same time interval, the 0- to 10-cm depth drops to a quasi-equilibrium, creating a second peak over the 50-cm average at approximately the end of the second day. Though the respiration rate of the top 0- to 10-cm interval drops substantially over the second day, it still contributes ~62% of the overall respiration at the end of the incubation. These observations illustrate that the majority of CO_2 is produced in the top 10 cm of this soil profile, with a transient response to a wetting event which is unique to the rest of the profile. This distinction is lost in the coarse incubation experiment. The rest of the soil profile, in contrast, may be reasonably constrained with careful mixing of an aggregated sample for incubation with minimal loss of information.

To simulate this high-resolution dataset from the second incubation, in comparison to the coarse shallow soil depth (0–52 cm) collected in the first experiment, we reoptimized the parameter sets in both the FO1 and DM2 models for the three subsets described in section 3.3 (Figure 12). Direct comparison of the

parameter values we used (Tables S4 and S5) shows that higher solubilization rates and decomposition rates are needed to simulate the top 0- to 10-cm interval for both the FO1 and DM2 models in comparison to the 0- to 50-cm aggregated values. These enhanced rates are anticipated given the high carbon content and dynamic nature of the shallowest soils. In addition, we found that the solubilization rates (which represent an ensemble of factors potentially limiting bioavailability of substrate carbon) necessary to simulate the remaining 10- to 50-cm depth interval must be approximately 2 orders of magnitude lower than that of the 0- to 10-cm interval to closely reproduce the delayed Birch type behavior. Though this lower solubilization rate is somewhat anticipated, such a large difference may be due to the following: (1) a lower enzyme activity at depth; (2) a larger amount of initial soluble carbon from root inputs near the surface; and (3) unique pathways and extents of transport limitation. Though the C/N ratios of the coarsely collected soil samples suggest no nitrogen limitation for microbial growth, the topmost soil layer might have different microbial functional groups with unique carbon use efficiency. This further suggests that the topmost soil layer should be treated separately in future model simulations if high-resolution depth-resolved respiration rates are needed. AIC values were calculated after reoptimizing the parameters of the two models as a means of further comparing their performance with the consideration of the complexity in the two modeling frameworks (Table 5). The AIC values indicate that the DM2 model still serves as a better method of predicting the CO_2 respiration rate of the top 10 cm of the soil profile compared to the FO1 model for this high-resolution dataset.

Notably, in this exercise, a slightly different parameter set was applied to the simulation of the respiration rate over the 0- to 50-cm interval acquired from reaveraging the high-resolution second incubation, compared to the one used to simulate the coarse 0- to 52-cm respiration data from the first incubation experiment. In particular, a slightly lower solubilization rate for the rapid microbial community and a higher solubilization rate for slow microbial community were used simulating the high-resolution second incubation dataset, with a lower Se_{half} value used for the slow microbial community. This distinct behavior highlights the effects of sampling and simulating datasets over coarser depth and time resolutions where high-resolution datasets are hard to acquire. In other words, this exercise can potentially guide us when applying smaller-scale models utilizing high-resolution dataset to larger-scale simulations, where most of the detailed information is lost. For these soils, we found that the distinction in Birch-type respiration peaks observed in the topsoil over short time intervals are lost in lower sampling frequency; thus, one may easily produce a simulation that misinterprets the respiration rates between the time points where data are measured. These errors could result in a biased estimation of the time span the soil microorganisms need to activate, which is critical if one is aiming at unraveling the detailed characteristic of a kind of operational taxonomic unit. From a modeling perspective, the usage of the coarse dataset for calibration could result in biased production rates of the soil substrate carbon and half saturation constant for the specific microbial population. However, we have also shown that such detailed information has little effect on the overall respiration estimation spanning multiple days. This is illustrated by the close comparison in the integrated respiration rate at the end of the first, second, and third days, indicating that the original coarse dataset with low time resolution is sufficient in a long-term (i.e., weekly or longer) simulation. In addition, this study has shown that the thin section of soil at the top of this profile contributes over 60% of the CO_2 respired, suggesting that an estimation of the respiration rate of a soil profile can be roughly made based on the information of its surface combined with an aggregated estimate of the deeper soil. Last but not least, the AIC values calculated from the simulations of the two different modeling structures show that the DM2 model serves as a better tool of predicting soil respiration rates across all scales considered.

4.4. Future Directions

Another potentially significant factor is the time span over which *Se* changes during a wetting or drying event. Shifts in the *Se* values in the current study were implemented as an instantaneous change from 0 to a certain value at the beginning of the incubation. Though this is valid for the present experimental design, a gradual increase of *Se* from low to high is commonly observed in reality as the result of extended and compounding periods of precipitation and dry out (Borken et al., 2003). Based on the equations developed herein, we note that such a time-dependent change in *Se* can support a transient increase in respiration rate using the first-order model (i.e., the monotonic nature shown here would be alleviated). However, this would still omit the lagged respiration peak generated using the dormancy model. Such cases require further

testing, as would be provided by a direct comparison of the performance of two models simulating one identical dataset from in situ measurements over multiple precipitation events. This will be addressed in subsequent studies using the East River Watershed datasets.

Finally, before applying the two models to in situ measurements, we recognize that the effects of transport limitation in such dynamic hydrologic settings are vital and still missing from the current laboratory-based study. In particular, a fixed O_2 concentration is set throughout the simulations, assuming O_2 is not a limiting factor below 66% *Se*, yet we observed some minor indication of oxygen limitation at near saturated conditions in our incubation dataset. Previous studies have shown that in natural environments, respiration can be limited by low O_2 concentration resulting from low replenishment rates at high *Se* (equations (10)–(12)) in that gas diffusion is negatively correlated with *Se* (e.g., Pingintha et al., 2010). As such, our current model could potentially overestimate the respiration rate at an effective saturation higher than 66%. In addition, since we are using a single solubilization rate as a summation of all the different processes that generate bioavailable carbon in the current study, this model cannot parse out the relative contribution of those processes such as absorption/desorption and other physical carbon protection pathways that can potentially influence the respiration rate of soil microbes. Moreover, a number of other processes affect CO_2 concentration in the subsurface, including carbonate weathering (induced by both carbonic acid and sulfuric acid) may further complicate the direct application of this model to estimate surface fluxes (Sánchez-Cañete et al., 2018; Winnick et al., 2017). These complexities may be addressed by expansion of the process-based dormancy modeling approach (equations (6)–(9) and (10)–(12)) into a reactive-transport modeling framework capable of linking the reaction network to gas and fluid phase transport, fluid-rock interaction, as well as absorption/desorption across intact soil columns (Steefel & Maher, 2009). Future work will include the collection of depth-resolved in situ soil CO_2 concentration data at the field site where our soil samples are collected, which will allow us to expand the current model to a 1-D reactive transport framework for the intact soil column.

5. Conclusions

An adjusted form of the reaction network developed by Manzoni et al. (2014), referred to as the dormancy model, was built and compared against a widely applied first-order model using two experimental datasets with different temporal and spatial resolutions. The first coarse dataset is assumed to broadly represent both moisture-respiration relationships and the Birch effects observed in many soils, while the other features high-resolution depth and sampling frequency. With an adjustment that allows the activation of unique microbial communities at distinct effective saturations in the structure of dormancy model, we evaluated FO1 and DM2 with consideration of both the quantity of the parameters and their ability to reproduce the two sets of experimental data. As a result, we conclude that despite the better performance of FO1 while simulating the decomposition of deep soil organic carbon (below 1 m), the implementation of moisture-dependent activation and dormancy rates provides an improved means of quantifying and predicting soil carbon respiration of a soil column under dynamic hydrologic conditions in both high- and low-resolution depths and sampling frequencies. This is particularly relevant to simulating the temporal patterns of Birch-type effects. In addition, we found that though the high-resolution dataset uniquely provides detailed information regarding the distinct behavior of the upper soil surface, a coarse dataset is sufficient for longer-term aggregated simulations spanning many days or longer.

Acknowledgments
This work is supported by the U.S. Department of Energy, Office of Science, Office of Biological and Environmental Research, under Awards DE-SC0014556 and DE-SC0018155. The authors wish to thank Michael Masters and Robert Sanford at the University of Illinois at Urbana–Champaign for valuable support during the incubation experiements, and Rose Abramoff at the Lawerence Berkeley National Lab for providing an internal USGS review. The authors declare that they have no conflict of interest. All measured datasets are reported within the body of this paper and are available on a GitHub repository (https://github.com/two2cold/Soil_respiration.git). Matlab scripts developed for the First Order, Dormancy, and AIC calculations are also accessible on the GitHub repository (https://github.com/two2cold/Soil_respiration.git).

References

Abramoff, R. Z., Davidson, E. A., & Finzi, A. C. (2017). A parsimonious modular approach to building a mechanistic belowground carbon and nitrogen model. *Journal of Geophysical Research: Biogeosciences*, *122*, 2418–2434. https://doi.org/10.1002/2017JG003796

Akaike, H. (1998). Information theory and an extension of the maximum likelihood principle. In E. Parzen, K. Tanabe, & G. Kitagawa (Eds.), *Selected Papers of Hirotugu Akaike* (pp. 199–213). New York, NY: Springer New York. https://doi.org/10.1007/978-1-4612-1694-0_15

Andrews, J. H., & Harris, R. F. (1986). r- and K-selection and microbial ecology. In K. C. Marshall (Ed.), *Advances in microbial ecology* (pp. 99–147). Boston, MA: Springer US. https://doi.org/10.1007/978-1-4757-0611-6_3

Bååth, E., & Anderson, T.-H. (2003). Comparison of soil fungal/bacterial ratios in a pH gradient using physiological and PLFA-based techniques. *Soil Biology and Biochemistry*, *35*(7), 955–963. https://doi.org/10.1016/S0038-0717(03)00154-8

Barnard, R. L., Osborne, C. A., & Firestone, M. K. (2015). Changing precipitation pattern alters soil microbial community response to wet-up under a Mediterranean-type climate. *ISME Journal*, *9*(4), 946–957. https://doi.org/10.1038/ismej.2014.192

Barnard, R. L., Osborne, C. A., & Firestone, M. K. (2013). Responses of soil bacterial and fungal communities to extreme desiccation and rewetting. *ISME Journal*, *7*(11), 2229–2241. https://doi.org/10.1038/ismej.2013.104

Batjes, N. H. (1996). Total carbon and nitrogen in the soils of the world. *European Journal of Soil Science*, *47*(2), 151–163. https://doi.org/10.1111/j.1365-2389.1996.tb01386.x

Bellamy, P. H., Loveland, P. J., Bradley, R. I., Lark, R. M., & Kirk, G. J. D. (2005). Carbon losses from all soils across England and Wales 1978-2003. *Nature*, *437*(7056), 245–248. https://doi.org/10.1038/nature04038

Birch, H. F. (1958). Pattern of humus decomposition in East African soils. *Nature*, *181*(4611), 788–788. https://doi.org/10.1038/181788a0

Birch, H. F. (1960). Nitrification in soils after different periods of dryness. *Plant and Soil*, *12*(1), 81–96. https://doi.org/10.1007/BF01377763

Birch, H. F. (1964). Mineralisation of plant nitrogen following alternate wet and dry conditions. *Plant and Soil*, *20*(1), 43–49. https://doi.org/10.1007/BF01378096

Blagodatskaya, E., & Kuzyakov, Y. (2013). Active microorganisms in soil: Critical review of estimation criteria and approaches. *Soil Biology and Biochemistry*, *67*, 192–211. https://doi.org/10.1016/j.soilbio.2013.08.024

Blankinship, J. C., Becerra, C. A., Schaeffer, S. M., & Schimel, J. P. (2014). Separating cellular metabolism from exoenzyme activity in soil organic matter decomposition. *Soil Biology and Biochemistry*, *71*, 68–75. https://doi.org/10.1016/j.soilbio.2014.01.010

Blazewicz, S. J., Schwartz, E., & Firestone, M. K. (2014). Growth and death of bacteria and fungi underlie rainfall-induced carbon dioxide pulses from seasonally dried soil. *Ecology*, *95*(5), 1162–1172. https://doi.org/10.1890/13-1031.1

Borken, W., Davidson, E. A., Savage, K., Gaudinski, J., & Trumbore, S. E. (2003). Drying and wetting effects on carbon dioxide release from organic horizons. *Soil Science Society of America Journal*, *67*(6), 1888–1896. https://doi.org/10.2136/sssaj2003.1888

Borken, W., & Matzner, E. (2009). Reappraisal of drying and wetting effects on C and N mineralization and fluxes in soils. *Global Change Biology*, *15*(4), 808–824. https://doi.org/10.1111/j.1365-2486.2008.01681.x

Bowen, G. J., & Beerling, D. J. (2004). An integrated model for soil organic carbon and CO2: Implications for paleosol carbonate pCO2 paleobarometry. *Global Biogeochemical Cycles*, *18*, GB1026. https://doi.org/10.1029/2003GB002117

Boyer, J. N., & Groffman, P. M. (1996). Bioavailability of water extractable organic carbon fractions in forest and agricultural soil profiles. *Soil Biology and Biochemistry*, *28*(6), 783–790. https://doi.org/10.1016/0038-0717(96)00015-6

Brockett, B. F. T., Prescott, C. E., & Grayston, S. J. (2012). Soil moisture is the major factor influencing microbial community structure and enzyme activities across seven biogeoclimatic zones in western Canada. *Soil Biology and Biochemistry*, *44*(1), 9–20. https://doi.org/10.1016/j.soilbio.2011.09.003

Brooks, R. H., & Corey, A. T. (1964). Hydraulic Properties of Porous Media and Their Relation to Drainage Design. *Transactions of the ASAE*, *7*(1), 0026–0028. https://doi.org/10.13031/2013.40684

Cable, J. M., Ogle, K., Williams, D. G., Weltzin, J. F., & Huxman, T. E. (2008). Soil texture drives responses of soil respiration to precipitation pulses in the Sonoran Desert: Implications for climate change. *Ecosystems*, *11*(6), 961–979. https://doi.org/10.1007/s10021-008-9172-x

Cabon, F., Girard, G., & Ledoux, E. (1991). Modelling of the nitrogen cycle in farm land areas. In J. J. R. Groot, P. de Willigen, & E. L. J. Verberne (Eds.), *Nitrogen turnover in the soil-crop system: Modelling of biological transformations, transport of nitrogen and nitrogen use efficiency. Proceedings of a Workshop held at the Institute for Soil Fertility Research, Haren, The Netherlands, 5–6 June 1990* (pp. 161–169). Dordrecht: Springer Netherlands. https://doi.org/10.1007/978-94-011-3434-7_3

Canarini, A., & Dijkstra, F. A. (2015). Dry-rewetting cycles regulate wheat carbon rhizodeposition, stabilization and nitrogen cycling. *Soil Biology and Biochemistry*, *81*, 195–203. https://doi.org/10.1016/j.soilbio.2014.11.014

Carbone, M. S., Still, C. J., Ambrose, A. R., Dawson, T. E., Williams, A. P., Boot, C. M., et al. (2011). Seasonal and episodic moisture controls on plant and microbial contributions to soil respiration. *Oecologia*, *167*(1), 265–278. https://doi.org/10.1007/s00442-011-1975-3

Chantigny, M. H. (2003). Dissolved and water-extractable organic matter in soils: A review on the influence of land use and management practices. *Ecological Aspects of Dissolved Organic Matter in Soils*, *113*(3), 357–380. https://doi.org/10.1016/S0016-7061(02)00370-1

Chen, X., Post, W. M., Norby, R. J., & Classen, A. T. (2011). Modeling soil respiration and variations in source components using a multi-factor global climate change experiment. *Climatic Change*, *107*(3-4), 459–480. https://doi.org/10.1007/s10584-010-9942-2

Cleveland, C. C., Nemergut, D. R., Schmidt, S. K., & Townsend, A. R. (2007). Increases in soil respiration following labile carbon additions linked to rapid shifts in soil microbial community composition. *Biogeochemistry*, *82*(3), 229–240. https://doi.org/10.1007/s10533-006-9065-z

Cook, F. J., & Knight, J. H. (2003). Oxygen transport to plant roots: Modeling for physical understanding of soil aeration. *Soil Science Society of America Journal*, *67*(1), 20–31. https://doi.org/10.2136/sssaj2003.2000

Cross, A., & Sohi, S. P. (2011). The priming potential of biochar products in relation to labile carbon contents and soil organic matter status. *Soil Biology and Biochemistry*, *43*(10), 2127–2134. https://doi.org/10.1016/j.soilbio.2011.06.016

Davidson, E. A., Belk, E., & Boone, R. D. (1998). Soil water content and temperature as independent or confounded factors controlling soil respiration in a temperate mixed hardwood forest. *Global Change Biology*, *4*(2), 217–227. https://doi.org/10.1046/j.1365-2486.1998.00128.x

Davidson, E. A., Samanta, S., Caramori, S. S., & Savage, K. (2012). The dual Arrhenius and Michaelis–Menten kinetics model for decomposition of soil organic matter at hourly to seasonal time scales. *Global Change Biology*, *18*(1), 371–384. https://doi.org/10.1111/j.1365-2486.2011.02546.x

Davidson, E. A., Savage, K. E., & Finzi, A. C. (2014). A big-microsite framework for soil carbon modeling. *Global Change Biology*, *20*(12), 3610–3620. https://doi.org/10.1111/gcb.12718

Dorodnikov, M., Blagodatskaya, E., Blagodatsky, S., Fangmeier, A., & Kuzyakov, Y. (2009). Stimulation of r- vs. K-selected microorganisms by elevated atmospheric CO_2 depends on soil aggregate size. *FEMS Microbiology Ecology*, *69*(1), 43–52. https://doi.org/10.1111/j.1574-6941.2009.00697.x

Einola, J.-K. M., Kettunen, R. H., & Rintala, J. A. (2007). Responses of methane oxidation to temperature and water content in cover soil of a boreal landfill. *Soil Biology and Biochemistry*, *39*(5), 1156–1164. https://doi.org/10.1016/j.soilbio.2006.12.022

Elberling, B. (2003). Seasonal trends of soil CO_2 dynamics in a soil subject to freezing. *Journal of Hydrology*, *276*(1–4), 159–175. https://doi.org/10.1016/S0022-1694(03)00067-2

Euskirchen, E. S., Chen, J., Gustafson, E. J., & Ma, S. (2003). Soil respiration at dominant patch types within a managed northern Wisconsin landscape. *Ecosystems*, *6*(6), 595–607. https://doi.org/10.1007/PL00021505

Evans, S. E., & Wallenstein, M. D. (2014). Climate change alters ecological strategies of soil bacteria. *Ecology Letters*, *17*(2), 155–164. https://doi.org/10.1111/ele.12206

Falk, M., Paw, U. K. T., Wharton, S., & Schroeder, M. (2005). Is soil respiration a major contributor to the carbon budget within a Pacific Northwest old-growth forest? *Agricultural and Forest Meteorology*, *135*(1–4), 269–283. https://doi.org/10.1016/j.agrformet.2005.12.005

Fan, Z., Neff, J. C., & Hanan, N. P. (2015). Modeling pulsed soil respiration in an African savanna ecosystem. *Agricultural and Forest Meteorology*, *200*, 282–292. https://doi.org/10.1016/j.agrformet.2014.10.009

Gabriel, C.-E., & Kellman, L. (2014). Investigating the role of moisture as an environmental constraint in the decomposition of shallow and deep mineral soil organic matter of a temperate coniferous soil. *Soil Biology and Biochemistry*, *68*, 373–384. https://doi.org/10.1016/j.soilbio.2013.10.009

Geisseler, D., Horwath, W. R., & Scow, K. M. (2011). Soil moisture and plant residue addition interact in their effect on extracellular enzyme activity. *Pedobiologia*, *54*(2), 71–78. https://doi.org/10.1016/j.pedobi.2010.10.001

Göransson, H., Godbold, D. L., Jones, D. L., & Rousk, J. (2013). Bacterial growth and respiration responses upon rewetting dry forest soils: Impact of drought-legacy. *Soil Biology and Biochemistry*, *57*, 477–486. https://doi.org/10.1016/j.soilbio.2012.08.031

Gorissen, A., Tietema, A., Joosten, N. N., Estiarte, M., Peuelas, J., Sowerby, A., et al. (2004). Climate change affects carbon allocation to the soil in shrublands. *Ecosystems*, *7*(6), 650–661. https://doi.org/10.1007/s10021-004-0218-4

Grant, R. F., & Rochette, P. (1994). Soil microbial respiration at different water potentials and temperatures: Theory and mathematical modeling. *Soil Science Society of America Journal*, *58*(6), 1681–1690. https://doi.org/10.2136/sssaj1994.03615995005800060015x

Grundmann, G. L., Renault, P., Rosso, L., & Bardin, R. (1995). Differential effects of soil water content and temperature on nitrification and aeration. *Soil Science Society of America Journal*, *59*(5), 1342–1349. https://doi.org/10.2136/sssaj1995.03615995005900050021x

Gusman, A. J., & Mariño, M. A. (1999). Analytical modeling of nitrogen dynamics in soils and ground water. *Journal of Irrigation and Drainage Engineering*, *125*(6), 330–337. https://doi.org/10.1061/(ASCE)0733-9437(1999)125:6(330)

Hao, Y., Nianpeng, H., Shenggong, L., Guirui, Y., Yang, G., & Ruomeng, W. (2016). Impact of land cover on temperature and moisture sensitivity of soil organic matter mineralization in subtropical southeastern China. *Journal of Resources and Ecology*, *7*(2), 85–91. https://doi.org/10.5814/j.issn.1674-764x.2016.02.002

Harmon, M. E. (2009). Woody detritus mass and its contribution to carbon dynamics of old-growth forests: The temporal context. In C. Wirth, G. Gleixner, & M. Heimann (Eds.), *Old-growth forests: Function, fate and value* (pp. 159–190). Berlin, Heidelberg: Springer Berlin Heidelberg. Retrieved from. https://doi.org/10.1007/978-3-540-92706-8_8

Harmon, M. E., Bond-Lamberty, B., Tang, J., & Vargas, R. (2011). Heterotrophic respiration in disturbed forests: A review with examples from North America. *Journal of Geophysical Research*, *116*, G00K04. https://doi.org/10.1029/2010JG001495

Harte, J., Torn, M. S., Chang, F.-R., Feifarek, B., Kinzig, A. P., Shaw, R., & Shen, K. (1995). Global warming and soil microclimate: Results from a meadow-warming experiment. *Ecological Applications*, *5*(1), 132–150. https://doi.org/10.2307/1942058

Hashimoto, S., & Komatsu, H. (2006). Relationships between soil CO_2 concentration and CO_2 production, temperature, water content, and gas diffusivity: implications for field studies through sensitivity analyses. *Journal of Forest Research*, *11*(1), 41–50. https://doi.org/10.1007/s10310-005-0185-4

Heiri, O., Lotter, A. F., & Lemcke, G. (2001). Loss on ignition as a method for estimating organic and carbonate content in sediments: Reproducibility and comparability of results. *Journal of Paleolimnology*, *25*(1), 101–110. https://doi.org/10.1023/A:1008119611481

Howard, D. M., & Howard, P. J. A. (1993). Relationships between co2 evolution, moisture content and temperature for a range of soil types. *Soil Biology and Biochemistry*, *25*(11), 1537–1546. https://doi.org/10.1016/0038-0717(93)90008-Y

Husen, E., Salma, S., & Agus, F. (2014). Peat emission control by groundwater management and soil amendments: Evidence from laboratory experiments. *Mitigation and Adaptation Strategies for Global Change*, *19*(6), 821–829. https://doi.org/10.1007/s11027-013-9526-3

Inglima, I., Alberti, G., Bertolini, T., Vaccari, F. P., Gioli, B., Miglietta, F., et al. (2009). Precipitation pulses enhance respiration of Mediterranean ecosystems: the balance between organic and inorganic components of increased soil CO_2 efflux. *Global Change Biology*, *15*(5), 1289–1301. https://doi.org/10.1111/j.1365-2486.2008.01793.x

Iovieno, P., & Bååth, E. (2008). Effect of drying and rewetting on bacterial growth rates in soil. *FEMS Microbiology Ecology*, *65*(3), 400–407. https://doi.org/10.1111/j.1574-6941.2008.00524.x

Jia, B., Zhou, G., & Yuan, W. (2007). Modeling and coupling of soil respiration and soil water content in fenced Leymus chinensis steppe, Inner Mongolia. *Ecological Modelling*, *201*(2), 157–162. https://doi.org/10.1016/j.ecolmodel.2006.09.008

Jin, X., Wang, S., & Zhou, Y. (2008). Microbial CO_2 production from surface and subsurface soil as affected by temperature, moisture, and nitrogen fertilisation. *Soil Research*, *46*(3), 273–280. https://doi.org/10.1071/SR07144

Kang, S., Doh, S., Lee, D., Lee, D., Jin, V. L., & Kimball, J. S. (2003). Topographic and climatic controls on soil respiration in six temperate mixed-hardwood forest slopes, Korea. *Global Change Biology*, *9*(10), 1427–1437. https://doi.org/10.1046/j.1365-2486.2003.00668.x

Kant, R., Ghosh, C., Singh, L., & Tripathi, N. (2011). Effect of bacterial and fungal abundance in soil on the emission of carbon dioxide from soil in semi-arid climate in India. In H. Gökçekus, U. Türker, & J. W. LaMoreaux (Eds.), *Survival and sustainability: Environmental concerns in the 21st century* (pp. 151–161). Berlin, Heidelberg: Springer Berlin Heidelberg. Retrieved from. https://doi.org/10.1007/978-3-540-95991-5_16

Kieft, T. L., Soroker, E., & Firestone, M. K. (1987). Microbial biomass response to a rapid increase in water potential when dry soil is wetted. *Soil Biology and Biochemistry*, *19*(2), 119–126. https://doi.org/10.1016/0038-0717(87)90070-8

Kim, D.-G., Mu, S., Kang, S., & Lee, D. (2010). Factors controlling soil CO_2 effluxes and the effects of rewetting on effluxes in adjacent deciduous, coniferous, and mixed forests in Korea. *Soil Biology and Biochemistry*, *42*(4), 576–585. https://doi.org/10.1016/j.soilbio.2009.12.005

Kirschbaum, M. U. F. (1995). The temperature dependence of soil organic matter decomposition, and the effect of global warming on soil organic C storage. *Soil Biology and Biochemistry*, *27*(6), 753–760. https://doi.org/10.1016/0038-0717(94)00242-S

Kleber, M., Nico, P. S., Plante, A., Filley, T., Kramer, M., Swanston, C., & Sollins, P. (2011). Old and stable soil organic matter is not necessarily chemically recalcitrant: implications for modeling concepts and temperature sensitivity. *Global Change Biology*, *17*(2), 1097–1107. https://doi.org/10.1111/j.1365-2486.2010.02278.x

Kumar, S., Ghotekar, Y. S., & Dadhwal, V. K. (2019). C-equivalent correction factor for soil organic carbon inventory by wet oxidation, dry combustion and loss on ignition methods in Himalayan region. *Journal of Earth System Science*, *128*(3), 62. https://doi.org/10.1007/s12040-019-1086-9

Lauber, C. L., Ramirez, K. S., Aanderud, Z., Lennon, J., & Fierer, N. (2013). Temporal variability in soil microbial communities across land-use types. *ISME Journal*, *7*(8), 1641–1650. https://doi.org/10.1038/ismej.2013.50

Lawrence, C. R., Neff, J. C., & Schimel, J. P. (2009). Does adding microbial mechanisms of decomposition improve soil organic matter models? A comparison of four models using data from a pulsed rewetting experiment. *Soil Biology and Biochemistry*, *41*(9), 1923–1934. https://doi.org/10.1016/j.soilbio.2009.06.016

Lellei-Kovács, E., Botta-Dukát, Z., de Dato, G., Estiarte, M., Guidolotti, G., Kopittke, G. R., et al. (2016). Temperature dependence of soil respiration modulated by thresholds in soil water availability across European Shrubland ecosystems. *Ecosystems*, *19*(8), 1460–1477. https://doi.org/10.1007/s10021-016-0016-9

Lennon, J. T., & Jones, S. E. (2011). Microbial seed banks: The ecological and evolutionary implications of dormancy. *Nature Reviews Microbiology*, *9*(2), 119–130. https://doi.org/10.1038/nrmicro2504

Li, X., Ishikura, K., Wang, C., Yeluripati, J., & Hatano, R. (2015). Hierarchical Bayesian models for soil CO_2 flux using soil texture: a case study in central Hokkaido, Japan. *Soil Science and Plant Nutrition*, *61*(1), 116–132. https://doi.org/10.1080/00380768.2014.978728

Li, Y., Xu, M., & Zou, X. (2006). Heterotrophic soil respiration in relation to environmental factors and microbial biomass in two wet tropical forests. *Plant and Soil*, *281*(1-2), 193–201. https://doi.org/10.1007/s11104-005-4249-1

Linn, D. M., & Doran, J. W. (1984). Effect of water-filled pore space on carbon dioxide and nitrous oxide production in tilled and nontilled soils 1. *Soil Science Society of America Journal*, *48*(6), 1267–1272.

Lloyd, J., & Taylor, J. A. (1994). On the temperature dependence of soil respiration. *Functional Ecology*, *8*(3), 315–323. https://doi.org/10.2307/2389824

Loeppert, R. H., & Suarez, D. L. (1996). Carbonate and gympusm. In Methods of soil analysis. Part 3. Chemical methods--SSSA (pp. 455–456). Madison, WI, USA: Soil Science Society of America and American Society of Agronomy.

Luo, Y., Ahlström, A., Allison, S. D., Batjes, N. H., Brovkin, V., Carvalhais, N., et al. (2016). Toward more realistic projections of soil carbon dynamics by Earth system models. *Global Biogeochemical Cycles*, *30*, 40–56. https://doi.org/10.1002/2015GB005239

Manzoni, S., Schaeffer, S. M., Katul, G., Porporato, A., & Schimel, J. P. (2014). A theoretical analysis of microbial eco-physiological and diffusion limitations to carbon cycling in drying soils. *Soil Biology and Biochemistry*, *73*, 69–83. https://doi.org/10.1016/j.soilbio.2014.02.008

Manzoni, S., Schimel, J. P., & Porporato, A. (2012). Responses of soil microbial communities to water stress: Results from a meta-analysis. *Ecology*, *93*(4), 930–938. https://doi.org/10.1890/11-0026.1

Markstrom, S. L., & Hay, L. E. (2009). Integrated Watershed Scale Response to Climate Change for Selected Basins Across the United States. *Water Resources IMPACT*, *11*(2), 8–10.

Martiny, A. C., Treseder, K., & Pusch, G. (2013). Phylogenetic conservatism of functional traits in microorganisms. *ISME Journal*, *7*(4), 830–838. https://doi.org/10.1038/ismej.2012.160

Meisner, A., Rousk, J., & Bååth, E. (2015). Prolonged drought changes the bacterial growth response to rewetting. *Soil Biology and Biochemistry*, *88*, 314–322. https://doi.org/10.1016/j.soilbio.2015.06.002

Mielnick, P. C., & Dugas, W. A. (2000). Soil CO_2 flux in a tallgrass prairie. *Soil Biology and Biochemistry*, *32*(2), 221–228. https://doi.org/10.1016/S0038-0717(99)00150-9

Miller, A. E., Schimel, J. P., Meixner, T., Sickman, J. O., & Melack, J. M. (2005). Episodic rewetting enhances carbon and nitrogen release from chaparral soils. *Soil Biology and Biochemistry*, *37*(12), 2195–2204. https://doi.org/10.1016/j.soilbio.2005.03.021

Moncrieff, J. B., & Fang, C. (1999). A model for soil CO_2 production and transport 2: Application to a Florida *Pinus elliotte* plantation. *Agricultural and Forest Meteorology*, *95*(4), 237–256. https://doi.org/10.1016/S0168-1923(99)00035-0

Monson, R. K., Lipson, D. L., Burns, S. P., Turnipseed, A. A., Delany, A. C., Williams, M. W., & Schmidt, S. K. (2006). Winter forest soil respiration controlled by climate and microbial community composition. *Nature*, *439*(7077), 711–714. https://doi.org/10.1038/nature04555

Moyano, F. E., Vasilyeva, N., Bouckaert, L., Cook, F., Craine, J., Curiel Yuste, J., et al. (2012). The moisture response of soil heterotrophic respiration: Interaction with soil properties. *Biogeosciences*, *9*(3), 1173–1182. https://doi.org/10.5194/bg-9-1173-2012

Moyano, F. E., Manzoni, S., & Chenu, C. (2013). Responses of soil heterotrophic respiration to moisture availability: An exploration of processes and models. *Soil Biology and Biochemistry*, *59*, 72–85. https://doi.org/10.1016/j.soilbio.2013.01.002

Niklińska, M., & Klimek, B. (2007). Effect of temperature on the respiration rate of forest soil organic layer along an elevation gradient in the Polish Carpathians. *Biology and Fertility of Soils*, *43*(5), 511–518. https://doi.org/10.1007/s00374-006-0129-y

Oikawa, P. Y., Grantz, D. A., Chatterjee, A., Eberwein, J. E., Allsman, L. A., & Jenerette, G. D. (2014). Unifying soil respiration pulses, inhibition, and temperature hysteresis through dynamics of labile soil carbon and O_2. *Journal of Geophysical Research: Biogeosciences*, *119*, 521–536. https://doi.org/10.1002/2013JG002434

Orchard, V. A., & Cook, F. J. (1983). Relationship between soil respiration and soil moisture. *Soil Biology and Biochemistry*, *15*(4), 447–453. https://doi.org/10.1016/0038-0717(83)90010-X

Paul, K. I., Polglase, P. J., O'Connell, A. M., Carlyle, J. C., Smethurst, P. J., & Khanna, P. K. (2003). Defining the relation between soil water content and net nitrogen mineralization. *European Journal of Soil Science*, *54*(1), 39–48. https://doi.org/10.1046/j.1365-2389.2003.00502.x

Persson, H., Von Fircks, Y., Majdi, H., & Nilsson, L. O. (1995). Root distribution in a Norway spruce (*Picea abies* (L.) Karst.) stand subjected to drought and ammonium-sulphate application. *Plant and Soil*, *168-169*(1), 161–165. https://doi.org/10.1007/BF00029324

Pingintha, N., Leclerc, M. Y., Beasley, J. P. Jr., Zhang, G., & Senthong, C. (2010). Assessment of the soil CO_2 gradient method for soil CO_2 efflux measurements: Comparison of six models in the calculation of the relative gas diffusion coefficient. *Tellus B*, *62*(1), 47–58. https://doi.org/10.1111/j.1600-0889.2009.00445.x

Placella, S. A., Brodie, E. L., & Firestone, M. K. (2012). Rainfall-induced carbon dioxide pulses result from sequential resuscitation of phylogenetically clustered microbial groups. *Proceedings of the National Academy of Sciences*, *109*(27), 10,931–10,936. https://doi.org/10.1073/pnas.1204306109

Porporato, A., D'Odorico, P., Laio, F., & Rodriguez-Iturbe, I. (2003). Hydrologic controls on soil carbon and nitrogen cycles. I. Modeling scheme. *Advances in Water Resources*, *26*(1), 45–58. https://doi.org/10.1016/S0309-1708(02)00094-5

Pumpanen, J., Ilvesniemi, H., & Hari, P. (2003). A process-based model for predicting soil carbon dioxide efflux and concentration. *Soil Science Society of America Journal*, *67*(2), 402–413. https://doi.org/10.2136/sssaj2003.4020

Reichstein, M., Rey, A., Freibauer, A., Tenhunen, J., Valentini, R., Banza, J., et al. (2003). Modeling temporal and large-scale spatial variability of soil respiration from soil water availability, temperature and vegetation productivity indices. *Global Biogeochemical Cycles*, *17*(4), 1104. https://doi.org/10.1029/2003GB002035

Rey, A., Petsikos, C., Jarvis, P. G., & Grace, J. (2005). Effect of temperature and moisture on rates of carbon mineralization in a Mediterranean oak forest soil under controlled and field conditions. *European Journal of Soil Science*, *56*(5), 589–599. https://doi.org/10.1111/j.1365-2389.2004.00699.x

Rumpel, C., & Kögel-Knabner, I. (2011). Deep soil organic matter—A key but poorly understood component of terrestrial C cycle. *Plant and Soil*, *338*(1-2), 143–158. https://doi.org/10.1007/s11104-010-0391-5

Sanaullah, M., Rumpel, C., Charrier, X., & Chabbi, A. (2012). How does drought stress influence the decomposition of plant litter with contrasting quality in a grassland ecosystem? *Plant and Soil*, *352*(1-2), 277–288. https://doi.org/10.1007/s11104-011-0995-4

Sánchez-Cañete, E. P., Barron-Gafford, G. A., & Chorover, J. (2018). A considerable fraction of soil-respired CO_2 is not emitted directly to the atmosphere. *Scientific Reports*, *8*(1), 13518. https://doi.org/10.1038/s41598-018-29803-x

Schimel, J. P., & Schaeffer, S. M. (2015). Microbial control over carbon cycling in soil. *The Causes and Consequences of Microbial Community Structure*, *22*, 155.

Schjønning, P., Thomsen, I. K., Moldrup, P., & Christensen, B. T. (2003). Linking soil microbial activity to water- and air-phase contents and diffusivities. *Soil Science Society of America Journal*, *67*(1), 156–165. https://doi.org/10.2136/sssaj2003.1560

Shi, A., & Marschner, P. (2014). Drying and rewetting frequency influences cumulative respiration and its distribution over time in two soils with contrasting management. *Soil Biology and Biochemistry*, *72*, 172–179. https://doi.org/10.1016/j.soilbio.2014.02.001

Skopp, J., Jawson, M. D., & Doran, J. W. (1990). Steady-state aerobic microbial activity as a function of soil water content. *Soil Science Society of America Journal*, *54*(6), 1619–1625. https://doi.org/10.2136/sssaj1990.03615995005400060018x

Steefel, C. I., & Maher, K. (2009). Fluid-rock interaction: A reactive transport approach. *Reviews in Mineralogy and Geochemistry*, *70*(1), 485–532. https://doi.org/10.2138/rmg.2009.70.11

Stevenson, L. H. (1977). A case for bacterial dormancy in aquatic systems. *Microbial Ecology*, *4*(2), 127–133. https://doi.org/10.1007/BF02014283

Tian, D., Wang, G., Yan, W., Xiang, W., & Peng, C. (2010). Soil respiration dynamics in *Cinnamomum camphora* forest and a nearby *Liquidambar formosana* forest in subtropical China. *Chinese Science Bulletin*, *55*(8), 736–743. https://doi.org/10.1007/s11434-009-0452-4

Trumbore, S. (2009). Radiocarbon and soil carbon dynamics. *Annual Review of Earth and Planetary Sciences*, *37*(1), 47–66. https://doi.org/10.1146/annurev.earth.36.031207.124300

Unger, S., Máguas, C., Pereira, J. S., David, T. S., & Werner, C. (2010). The influence of precipitation pulses on soil respiration—Assessing the "Birch effect" by stable carbon isotopes. *Soil Biology and Biochemistry*, *42*(10), 1800–1810. https://doi.org/10.1016/j.soilbio.2010.06.019

Vanhala, P. (2002). Seasonal variation in the soil respiration rate in coniferous forest soils. *Soil Biology and Biochemistry*, *34*(9), 1375–1379. https://doi.org/10.1016/S0038-0717(02)00061-5

Vanhala, P., Tamminen, P., & Fritze, H. (2005). Relationship between basal soil respiration rate, tree stand and soil characteristics in boreal forests. *Environmental Monitoring and Assessment*, *101*(1-3), 85–92. https://doi.org/10.1007/s10661-005-9134-0

Vanhala, P., Karhu, K., Tuomi, M., Björklöf, K., Fritze, H., & Liski, J. (2008). Temperature sensitivity of soil organic matter decomposition in southern and northern areas of the boreal forest zone. *Soil Biology and Biochemistry*, *40*(7), 1758–1764. https://doi.org/10.1016/j.soilbio.2008.02.021

Verburg, P. S. J., Larsen, J., Johnson, D. W., Schorran, D. E., & Arnone, J. A. (2005). Impacts of an anomalously warm year on soil CO_2 efflux in experimentally manipulated tallgrass prairie ecosystems. *Global Change Biology*, *11*(10), 1720–1732. https://doi.org/10.1111/j.1365-2486.2005.001032.x

Wagle, P., & Kakani, V. G. (2014). Confounding effects of soil moisture on the relationship between ecosystem respiration and soil temperature in switchgrass. *BioEnergy Research*, *7*(3), 789–798. https://doi.org/10.1007/s12155-014-9434-8

Wang, G., Jagadamma, S., Mayes, M. A., Schadt, C. W., Megan Steinweg, J., Gu, L., & Post, W. M. (2015). Microbial dormancy improves development and experimental validation of ecosystem model. *ISME Journal*, *9*(1), 226–237. https://doi.org/10.1038/ismej.2014.120

Wang, X., Li, X., Hu, Y., Lv, J., Sun, J., Li, Z., & Wu, Z. (2010). Effect of temperature and moisture on soil organic carbon mineralization of predominantly permafrost peatland in the Great Hing'an Mountains, Northeastern China. *Journal of Environmental Sciences*, *22*(7), 1057–1066. https://doi.org/10.1016/S1001-0742(09)60217-5

Welsch, D. L., & Hornberger, G. M. (2004). Spatial and temporal simulation of soil CO_2 concentrations in a small forested catchment in Virginia. *Biogeochemistry*, *71*(3), 413–434. https://doi.org/10.1023/B:BIOG.0000049350.24911.e9

Winnick, M. J., Carroll, R. W. H., Williams, K. H., Maxwell, R. M., Dong, W., & Maher, K. (2017). Snowmelt controls on concentration-discharge relationships and the balance of oxidative and acid-base weathering fluxes in an alpine catchment, East River, Colorado. *Water Resources Research*, *53*, 2507–2523. https://doi.org/10.1002/2016WR019724

Wu, H.-J., & Lee, X. (2011). Short-term effects of rain on soil respiration in two New England forests. *Plant and Soil*, *338*(1-2), 329–342. https://doi.org/10.1007/s11104-010-0548-2

Xu, L., Baldocchi, D. D., & Tang, J. (2004). How soil moisture, rain pulses, and growth alter the response of ecosystem respiration to temperature. *Global Biogeochemical Cycles*, *18*, GB4002. https://doi.org/10.1029/2004GB002281

Yan, L., Chen, S., Xia, J., & Luo, Y. (2014). Precipitation regime shift enhanced the rain pulse effect on soil respiration in a semi-arid steppe. *PLoS ONE*, *9*(8), e104217. https://doi.org/10.1371/journal.pone.0104217